Supporting Information

Reduced Water Activity in Co-Solvent Electrolyte Enables 2V Zinc-Ion Hybrid Capacitors with Prolonged Stability and High Energy Density

Ali Khosrozadeh[a, b], Miao Chang[b, c], Parisa Vahdatkhah[a], Jian Liu[b*], Oleksandr Voznyy[a*]

[a] *Department of Physical & Environmental Sciences, University of Toronto, Toronto, ON, M1C 1A4, Canada*

[b] *School of Engineering, Faculty of Applied Science, The University of British Columbia, Kelowna, BC, V1V 1V7, Canada*

[c] *School of Materials Science and Engineering, Huazhong University of Science and Technology, Wuhan, 430074, China*

[*] Corresponding authors. E-mail address: o.voznyy@utoronto.ca (O. Voznyy), jian.liu@ubc.ca (J. Liu).

Methods and Experimental Section

DFT-MD simulations

DFT-MD calculations were carried out using the QUICKSTEP module in CP2K [1] with molecularly optimized (MOLTOPT DZVP) basis set [2] and Godecker-Teter-Hutter pseudopotentials [3]. To obtain the electrolyte structure, the simulation cells (CELL_OPT) were optimized to achieve compact molecular packing, followed by 15,000-20,000 steps of MD simulations with a time step of 1 fs using the NVT ensemble (Nose-Hoover thermostat) at 300 K. The geometry optimization (GEO_OPT) was carried out after MD simulations.

To estimate the tendency of Zn^{2+}-bound water to deprotonate for representative Zn^{2+}-solvation shells in the Aq, Hyb and organic (with water additive) electrolytes, a proton from a bound water molecule was manually removed. The total energy difference was obtained from DFT calculations (geometry optimization) before and after removing the water proton. This process was repeated for few cases for each representative solvation shell (i.e., different hydrogens of water). An electrolyte has a higher "deprotonation tendency" when this energy difference is lower. It is note that the calculation of deprotonation energy should be made based on free energies [4, 5].

Structural characterizations

The ^{1}H and ^{17}O NMR spectra were acquired on Agilent DD2 600MHz spectrometer equipped with HFX 600MHz probe, by preparing the NMR samples in a 3 mm tube and then inserting it into a 5 mm tube containing a deuterated DMSO.

The porosity properties of the commercial activated carbon (AC30) were determined by conducting the nitrogen adsorption/desorption measurements at 77.3 K using Autosorb (Quantachrome Instruments). The specific surface area and the pore size distribution were obtained using the Brunauer-Emmett-Teller (BET) method and quenched solid density functional theory (QSDFT, slit pore) model, respectively. The porosity parameters were calculated using the weight of the sample (AC30) after undergoing outgassing at 200 °C for 98 h.

The surface morphology of samples was obtained using an SEM (Tescan Mira 3 XMU) and their elemental compositions were acquired using an EDS (X-Max detector, Oxford Instruments). XRD and

XPS patterns for Zn foils were recorded using Rigaku-Miniflex-6G diffractometer and Thermo Scientific K-Alpha, respectively. Prior to SEM, EDS, XRD, and XPS measurements, Zn foils were cleaned from glass fibers and washed with ethanol and water to remove residual salts.

Electrolyte preparation

To prepare hybrid electrolytes with different molar ratios (Table S1 and S2), a certain amount of $Zn(OTf)_2$ (zinc trifluoromethanesulfonate, >98%, TCI) was dissolved into a defined mixture of water/AN (≥99.9%, VWR). For example, the main electrolyte used in this study, with an optimized salt/water/AN molar ratio of 1:3.5:3.5 (denoted as Hyb), was prepared by using 6 g of salt, 1.04 g of water (water/salt molar ratio of 3.5), 2.37 of g AN (AN/salt molar ratio of 3.5). For comparison, 3M $Zn(OTf)_2$ in water (Aq) and 1M $Zn(OTf)_2$ in AN (Org) were also prepared (Table S1). The electrolyte preparation and cell assembly were carried out under an ambient environment, which is of practical importance due to the lower cost of scaling up for the manufacturing process.

Electrochemical characterizations

A commercial activated carbon (ASAC30, AdvEn Industries Inc.), denoted AC30, was used as the capacitor-type (storage by double-layer mechanism) active material for the ZIC cathode. AC30-based electrodes were prepared as follows. Briefly, 85 wt% AC30, 10 wt % of polytetrafluoroethylene (PTFE; 60 wt% water dispersion, MTI), and 5% acetylene black (AB; MTI) were well mixed in a mortar (and pestle) with the help of isopropanol. The paste was formed into a thin film using a manual roll-press. Then, the electrodes were punched out of the film in the form of round disks (diameter: 1.27 cm, unless stated otherwise). Each electrode was pressed onto a woven titanium mesh (diameter: 1.27 cm), followed by drying in an oven at 100 °C overnight.

ZICs were assembled in a two-electrode system (CR2032 coin cell, stainless steel 316) using the AC30-based electrode as the cathode and Zn metal foil (thickness: 150 µm, diameter: 1.4 cm) as the anode, separated by one separator (diameter: 1.9 cm, Whatman® glass microfiber, Grade GF/A). SCs were assembled in symmetric two-electrode systems (CR2032 coin cells) using the AC30-based electrodes and one cellulose separator (Whatman Grade 1). The volume of electrolytes used in the assembly of Hyb ZICs was 60 µL unless otherwise stated (e.g., 80 µL for the electrolyte study). For other electrolytes

(Aq, Org), 80 µL of the electrolyte was used in the investigations (electrolyte volume was found to have a negligible effect on the performance of ZICs with the Aq and Org electrolytes). All stainless-steel coin cells included one spring and two spacers (thickness: 0.75 mm). The areal mass loading of AC30 in the electrodes used for the assembly of ZICs and SCs was in the range of 2-4 mg/cm^2 (thickness: 0.20-0.22 mm) unless stated otherwise.

Similar to ZICs, Zn-Zn and Zn-Ti cells were assembled using CR2032 coin cells, Zn metal foil, glass fiber separator, and electrolyte volume of 80 µL (Aq, Hyb, Org). Two identical Zn foils (diameter: 1.4 cm) were used in the Zn-Zn symmetric cells. A Ti foil (diameter: 1.4 cm) as the working electrode and a Zn foil as both the reference and counter electrodes were used in Zn-Ti cells.

The electrochemical measurements were carried out using electrochemical workstations (SP-150 and VMP, BioLogic). The rate tests of ZICs included GCD tests (0.2-1.8 V, 0.3 to 150 mA), CV tests (0.2-1.8 V, scan rates ranging from 5 to 400 mV/s), and EIS (100 kHz to 0.01 Hz with an AC amplitude of 10 mV and zero DC amplitude). The minimum threshold of GCD current was defined as the current for which the coulombic efficiency starts to decrease. The GCD and CV tests of ZICs with Hyb and Org were also performed in the range of 0.2-2 V (0.5 mA was the minimum GCD current). The GCD cycling tests were carried out on a BTS battery tester (BTS-4008-5V-50mA, Neware) with no rest between the cycles.

The capacitive properties of ZICs were calculated based on GCD curves. The specific capacity (mAh/g) of ZICs was determined using the formula $C = I\Delta t/m$, where I is the discharge current, Δt is the discharge time after the potential drop, and m is the mass of activated carbon (AC30) in the cathode. The equivalent series resistance (ESR) was obtained from $ESR = V_{IR}/I$, where V_{IR} is the potential drop at the beginning of the discharge curve. The energy density (E, Wh/kg) and power density (P, kW/kg) were calculated by $E = (I/m)\int V dt$ and $P = E/\Delta t$, respectively. Current density (A/g) used in the plots was defined as I/m. The current in the CV curves was normalized to either current density (A/g) or capacitance (F/g) using $C_{\mathrm{cv}} = I/(mv)$, where v is the potential scan rate.

Table S1. Summary of main electrolytes prepared in this study.

Acronyms	Electrolyte	m (molality, mol kg^{-1})	Electrolyte density (g mL^{-1})	Electrolyte vol., salt mass used	H_2O/salt molar ratio	AN/salt molar ratio
Aq	3M $Zn(CF_3SO_3)_2$ in H_2O (1:14.2:0*)	3.91	1.9	5 mL, 5.45 g	14.2	0
Org	1M $Zn(CF_3SO_3)_2$ in AN (1:0:17.7*)	1.37	1.1	5 mL, 1.82 g	> 0**	17.7
Hyb	$Zn(CF_3SO_3)_2$ in H_2O/AN (1:3.5:3.5*)	4.84	1.4	6.8 mL, 6 g	3.5**	3.5

* Salt/H_2O/AN molar ratio to salt.

** Since the electrolytes were prepared under ambient atmosphere, a trace amount of water was adsorbed by the salt and AN. In the DFT-MD simulations of the Org electrolyte, H_2O/salt molar ratio was assumed to be 3, i.e., $Zn(CF_3SO_3)_2.3H_2O$.

It is noted that the estimated density of the Aq and Hyb electrolytes using the optimized size of periodic unit cells in the DFT simulations are 1.7 and 1.5 g/mL, which agree well with their measured density of 1.9 and 1.4 g/mL, respectively (Table S1). The Hyb and Org electrolytes have a lower density than the Aq one due to their bulkier solvation structure as a result of having fewer water molecules (or more AN molecules).

Table S2. Summary of other electrolytes prepared in this study.

Acronyms	Electrolyte	m (molality, mol/kg)
2M zinc sulfate	2M $ZnSO_4$ in H_2O	-
Hyb (1:3.8:3.8)	$Zn(CF_3SO_3)_2$ in H_2O/AN (1:3.8:3.8)	4.46
Hyb (1:3:4.6)	$Zn(CF_3SO_3)_2$ in H_2O/AN (1:3:4.6)	4.12
Hyb (1:4:3)	$Zn(CF_3SO_3)_2$ in H_2O/AN (1:4:3)	5.12

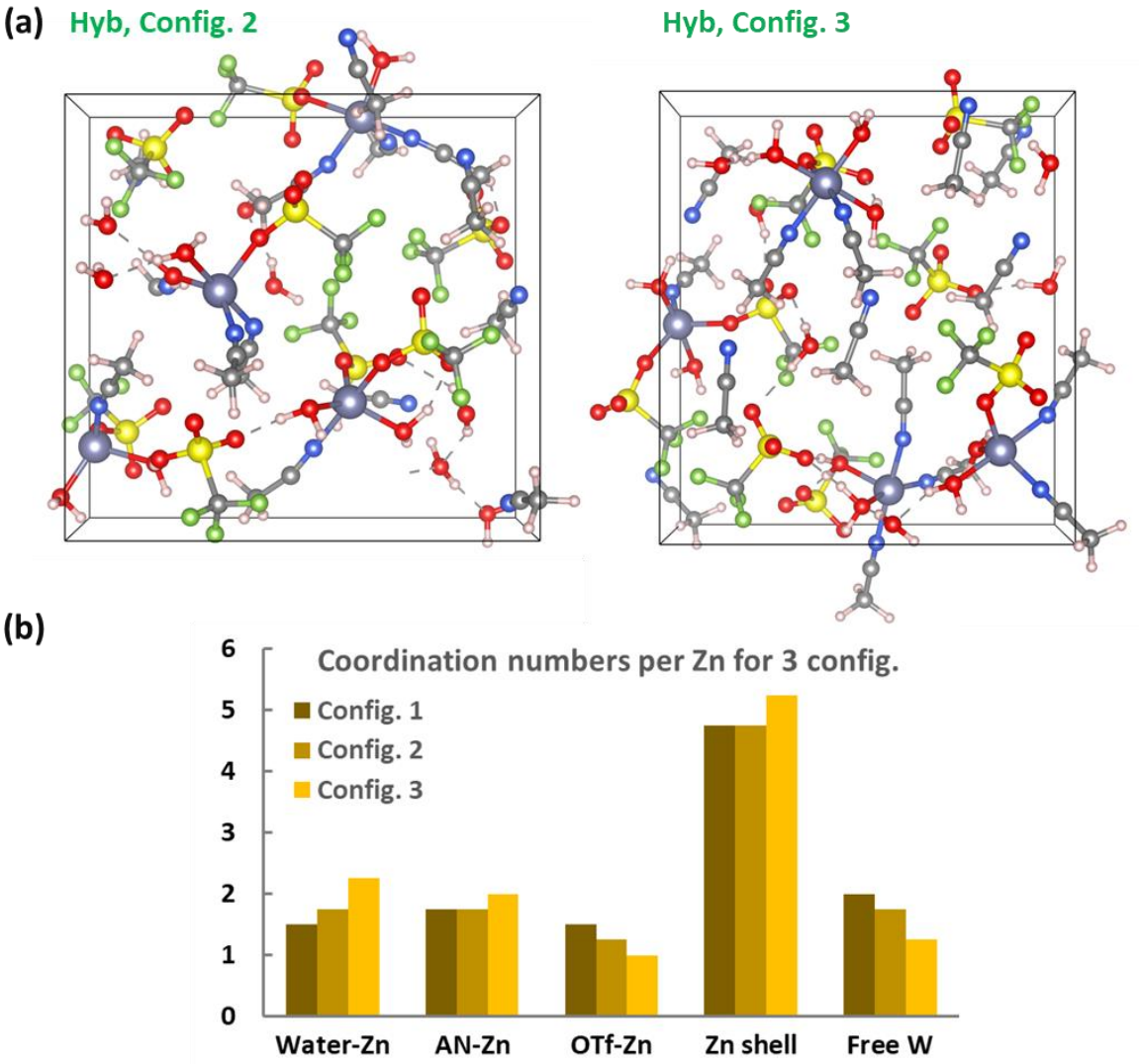

Figure S1. (a) Snapshots of the solvation structure of the Hyb electrolyte ($Zn(OTf)_2/(H_2O)_{3.5}/(AN)_{3.5}$) for 2 other initial configurations. (b) The summary of average coordination numbers per Zn^{2+} for the Hyb electrolyte with different initial configurations.

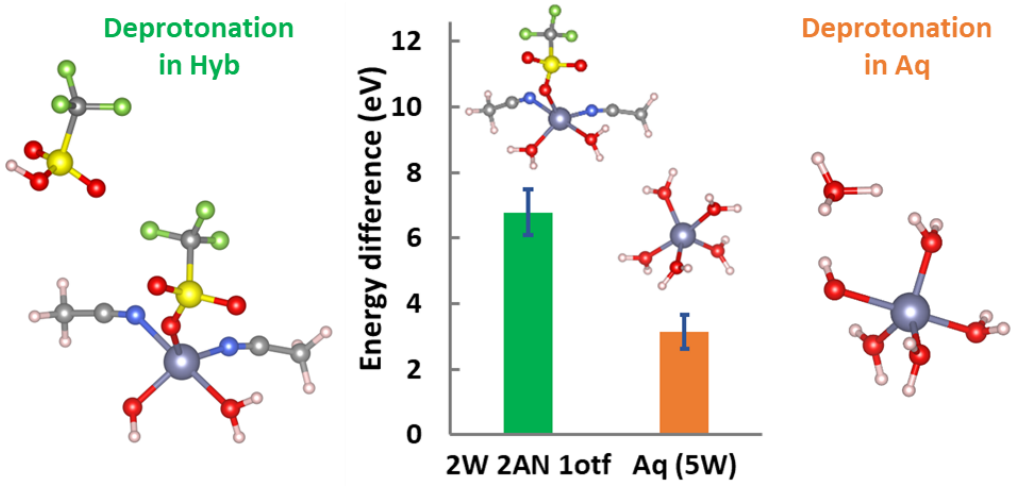

Figure S2. Comparative deprotonation energy of Zn^{2+}-bound water molecules obtained for the Aq and Hyb electrolytes using MD simulations. The representative snapshots display deprotonated water molecules, where the proton was attached to other species (surrounding environment in both electrolytes was hidden for better visualization.). To estimate the tendency of deprotonation in Zn^{2+}-bound water molecules in the electrolytes, one hydrogen from a Zn^{2+}-bound water molecule was manually relocated to another place in the simulation cell and allowed to attach to another molecule in the presence of other solvents and ions in the simulation box. The energy difference was calculated by the difference between the energy of the cell before and after 2,000 steps of MD simulations (Cons Qty: potential + kinetic energy). This process was repeated for few cases for each electrolyte (i.e., different hydrogens from water were relocated to different places).

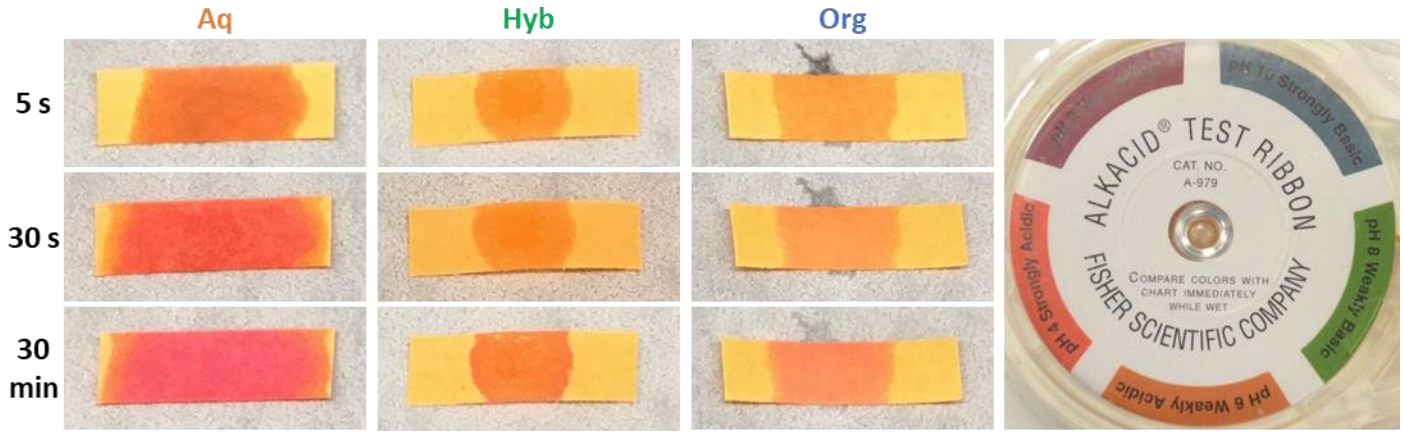

Figure S3. The visual comparison of the electrolyte acidity (Aq, Hyb, and Org) using a pH indicator.

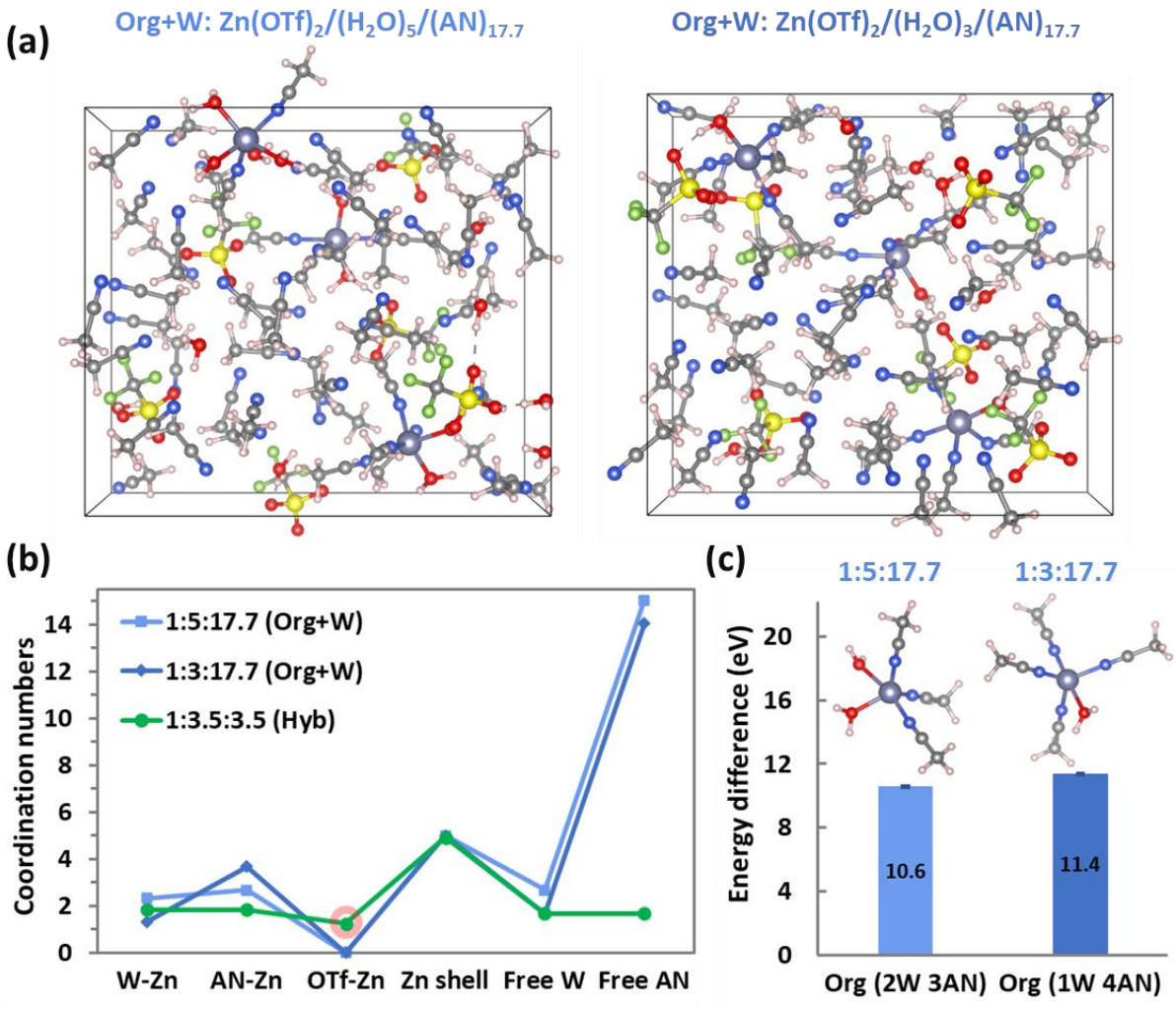

Figure S4. (a) Snapshots of the solvation structure of two dilute organic electrolytes (1M $Zn(OTf)_2$ in AN) with water additive (Org+W) with H_2O/salt molar ratios of 5 and 3: $Zn(OTf)_2/(H_2O)_5/(AN)_{17.7}$ and $Zn(OTf)_2/(H_2O)_3/(AN)_{17.7}$. (b) The coordination numbers per Zn^{2+} for two Org electrolytes are compared with that of Hyb electrolyte. (c) Comparison of the tendency for water coordinated with Zn^{2+} to deprotonate. The total energy difference obtained from DFT calculations (geometry optimization) before and after removing a water proton for representative Zn^{2+}-solvation shells in two Org electrolytes.

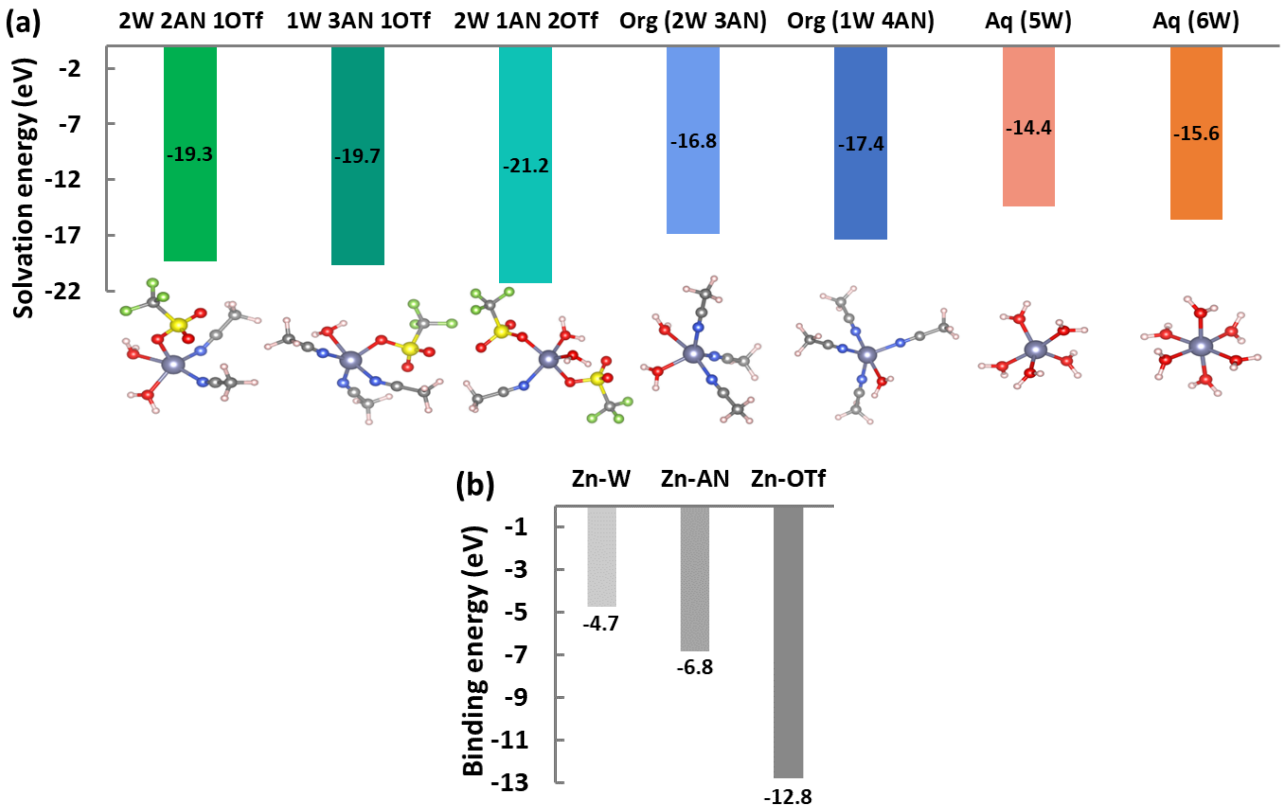

Figure S5. (a) Geometries and corresponding solvation energies for representative Zn^{2+}-solvation shells in the Hyb, Aq, and organic (with water additive) obtained from DFT calculations. The first three complexes are the major Zn^{2+}-solvation shells found in the Hyb electrolyte. (b) The binding energies calculated for $Zn^{2+}(H_2O)$, $Zn^{2+}(AN)$, and $Zn^{2+}(OTf^-)$.

The solvation energy for $Zn^{2+}[(H_2O)_x(AN)_y(OTf^-)_z]$ complex was calculated according to [6]:

$$E_{complex} = \mathrm{E}\left(\mathrm{Zn}^{2+}[(\mathrm{H_2O})_x(\mathrm{AN})_y(\mathrm{OTf}^-)_z]\right) - \mathrm{E}(\mathrm{Zn}^{2+}) - x\mathrm{E}(\mathrm{H_2O}) - y\mathrm{E}(\mathrm{AN}) - z\mathrm{E}(\mathrm{OTf}^-),$$

where E is the total energy of the unit in parenthesis, which is obtained from its geometry optimization (GEO_OPT); *x*, *y*, and *z* are the number of coordinating H_2O, AN, and OTf in the solvation shell of Zn^{2+}.

Characterization of activated carbon cathode:

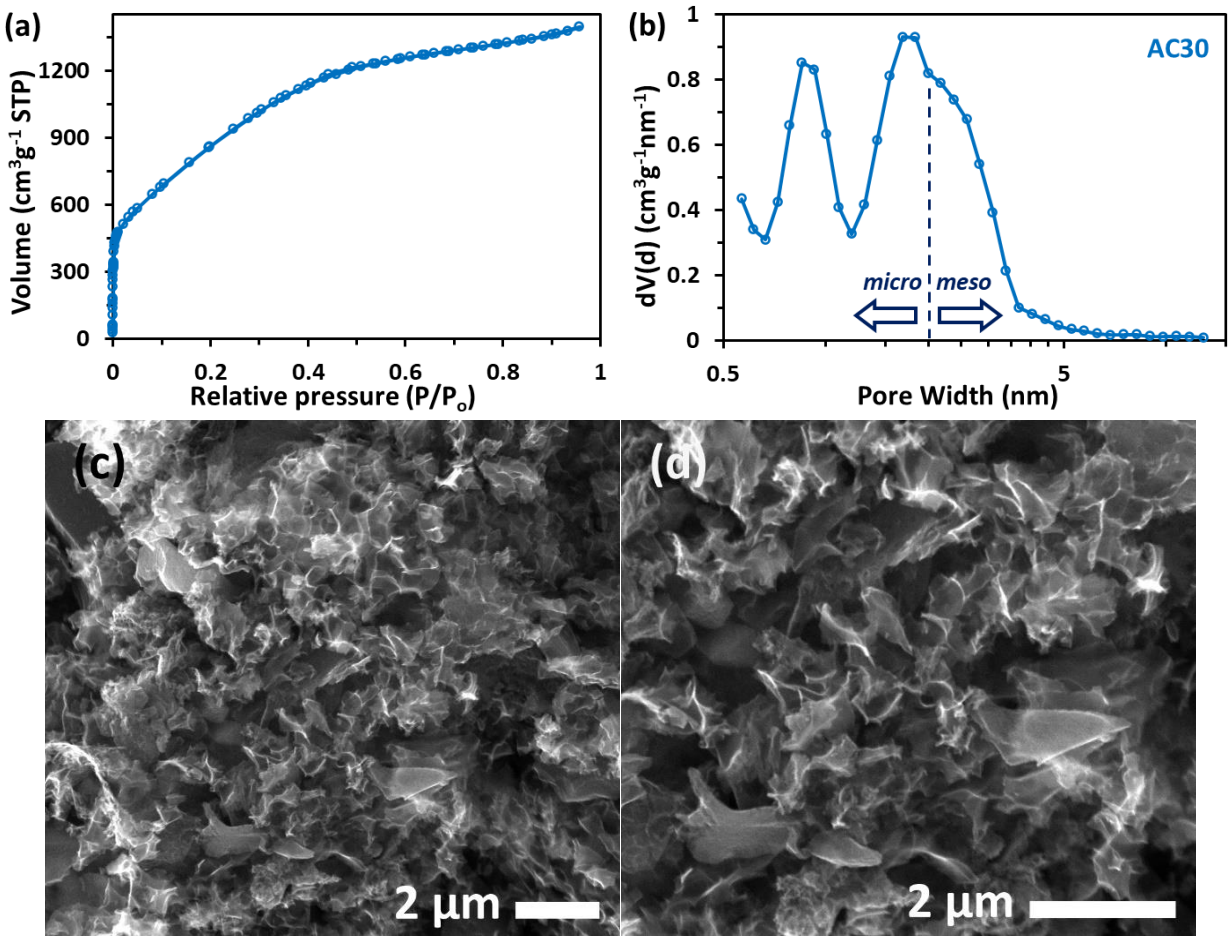

Figure S6. (a) Nitrogen adsorption/desorption isotherms and (b) pore size distribution (slit pore, QSDFT equilibrium model) of AC30 powder (ASAC30). (c and d) SEM images illustrate the macroporous morphology of AC30. This activated carbon has a hierarchical pore structure, including micro-, meso- and macropores. The macropores act as ion-buffering reservoirs and facilitate penetration for the bulk of the electrolyte into the electrode [7-9].

Table S3. Porosity properties of AC30.

S_{BET} (m^2/g)	Avg pore width (nm)	V_t (cm^3/g)	QSDFT V_t (cm^3/g)	QSDFT S_t (m^2/g)
3260	2.65	2.16	1.99	2471

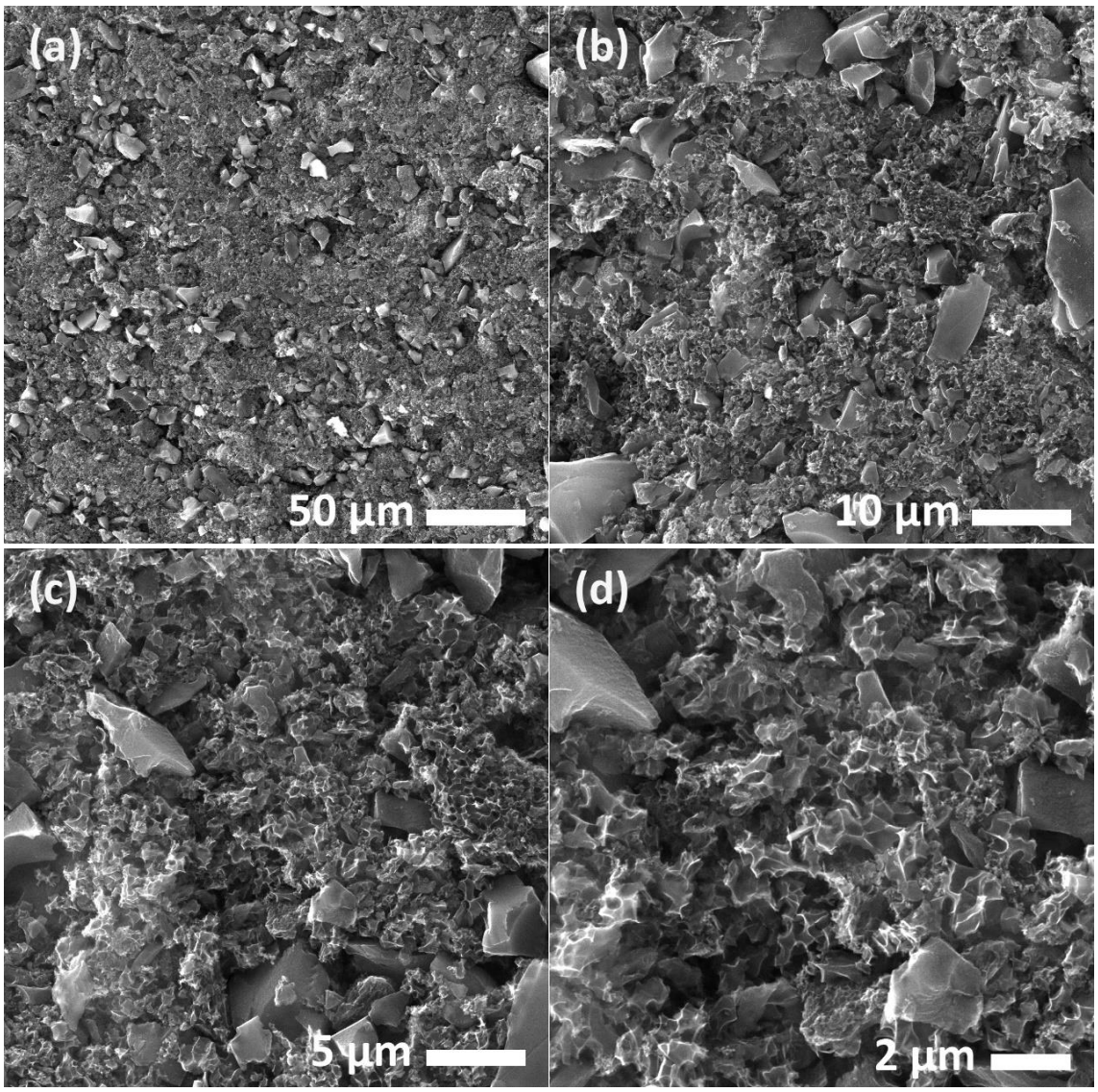

Figure S7. SEM images of PTFE-based AC30 electrode. The electrode density is about 0.19 (g/cm^3).

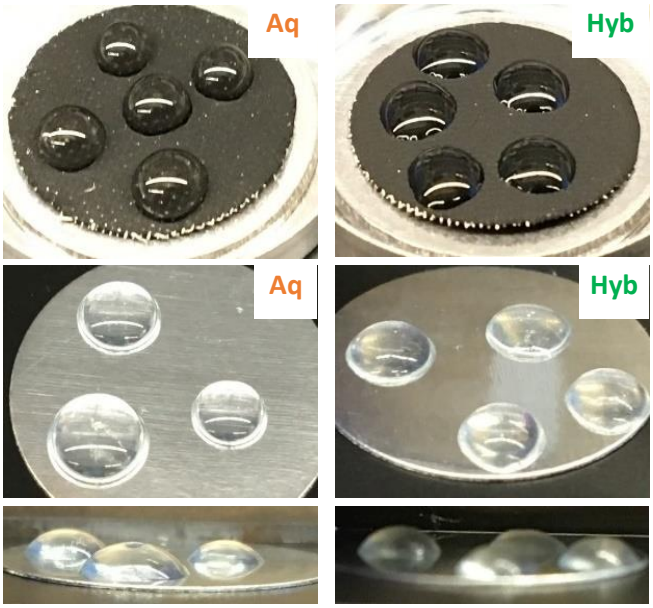

Figure S8. The visual comparison of electrolyte wetting. Photos were taken ~4 s after dropping electrolytes on the electrodes exhibiting the surface wettability for each electrolyte. The electrolyte drops were placed on the electrodes from approximately 1 mm distance using 200 µL pipette to obtain consistent results. The Hyb and Aq show a similar contact angle on Zn foil, but Hyb shows a much smaller contact angle on the AC30 electrode indicating its better wettability toward hydrophobic carbons.

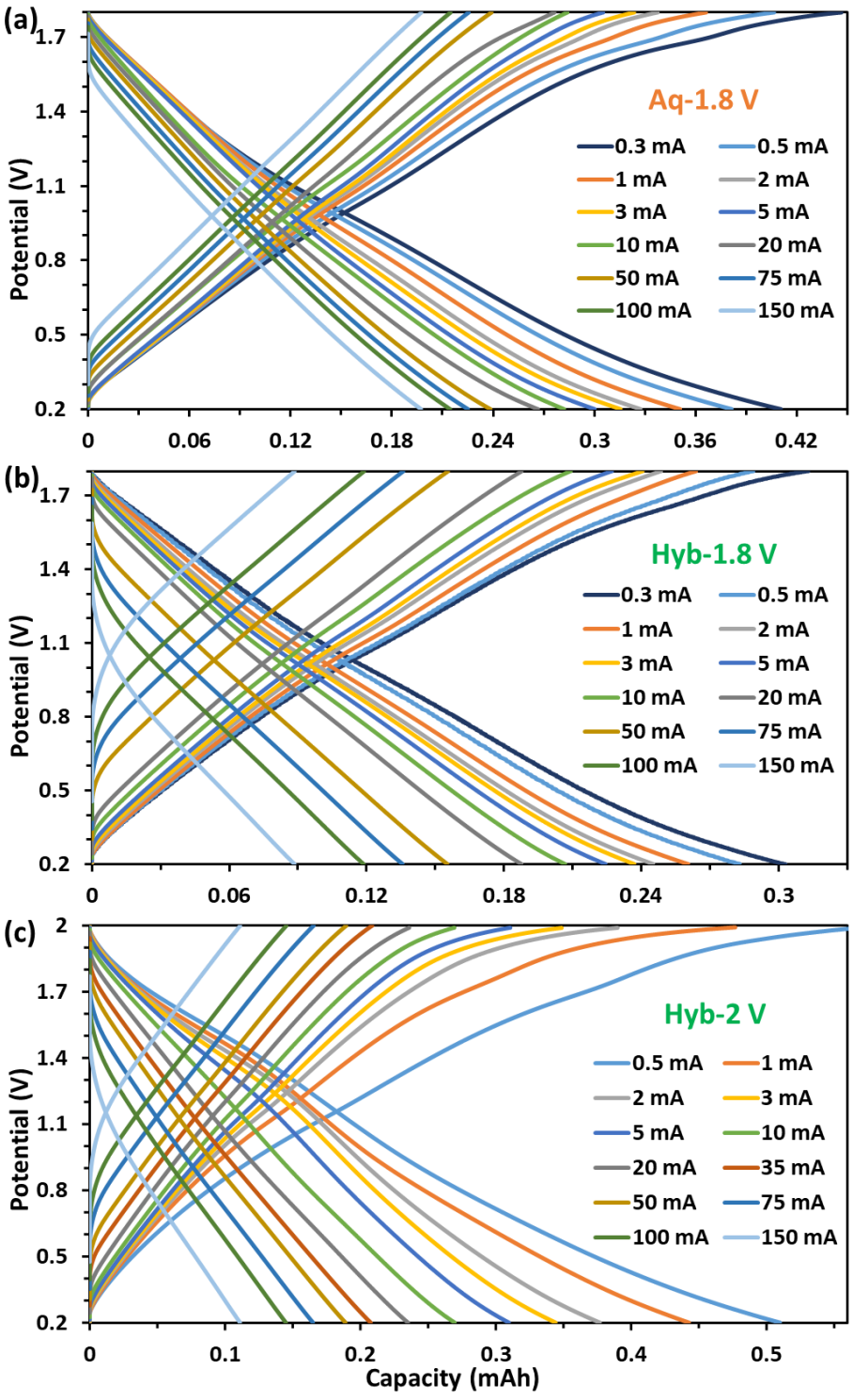
(a)
Aq-1.8 V
0.3 mA
0.5 mA
1 mA
2 mA
3 mA
5 mA
10 mA
20 mA
50 mA
75 mA
100 mA
150 mA
Potential (V)
(b)
Hyb-1.8 V
(c)
Hyb-2 V
35 mA
Capacity (mAh)

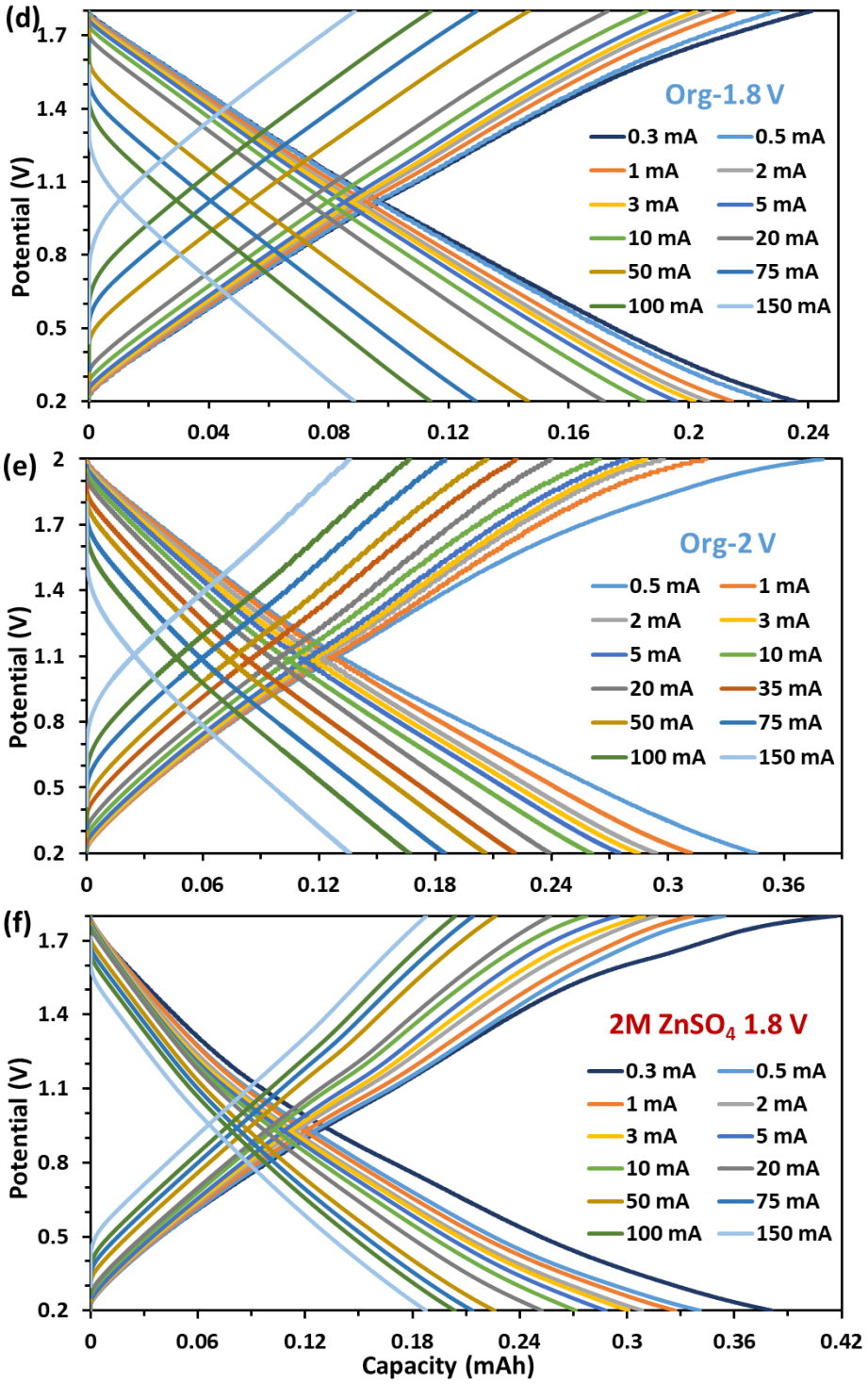

Figure S9. GCD curves used to evaluate the rate performance of fabricated ZICs with different electrolytes, i.e., Aq (0.2-1.8 V), Hyb (0.2-1.8 V and 0.2-2 V), Org (0.2-1.8 V and 0.2-2 V), and aqueous (2M $ZnSO_4$; 0.2-1.8 V). The GCD curves in (a-d) correspond to the ZICs shown Figure 3a-c, the curves in (d and e) correspond to the ZICs shown Figure S40a, and the curve in (f) corresponds to the ZIC (2M $ZnSO_4$) shown Figure S13. The mass loading of AC30 in the cathodes of ZICs are: Aq (2.62 mg/cm^2), Hyb (2.22 mg/cm^2), Org (2.15 mg/cm^2), and aqueous (2M $ZnSO_4$; 2.42 mg/cm^2).

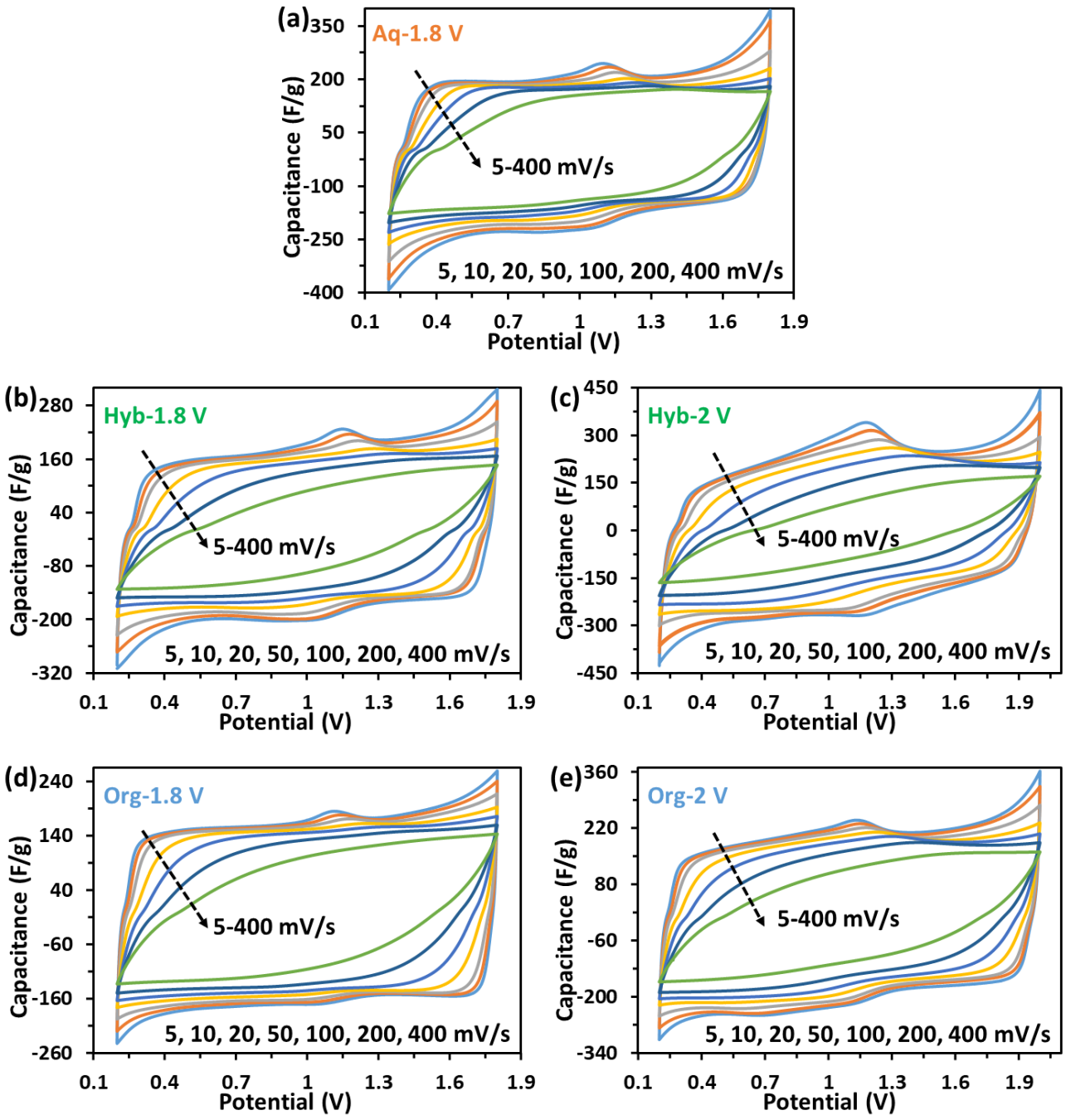

Figure S10. CV curves of ZICs fabricated with the Aq (0.2-1.8 V), Hyb (0.2-1.8 V and 0.2-2 V), and Org (0.2-1.8 V and 0.2-2 V) electrolytes. These CV curves correspond to the ZICs shown Figure 3a-c and Figure S9. The redox peaks at about 1.2 V and 1 V showing in the CV curves of ZICs correspond to the stripping/plating process of Zn/Zn^{2+} on the Zn anode.

The sharp rise in the capacitance (current) near the upper potential vertex in CV curves at a low rate is an indication of the water-splitting threshold [9], i.e., the competitive HER during Zn deposition in this case. This rise at the upper potential vertex in CV curves of Aq ZIC is sharper than those of Hyb and Org at 1.8 V (e.g., Figure 3c, Figure S10), which implies that the water-induced side reactions are more pronounced for Aq. The failure mechanism of an Aq ZIC is either a dendritic short or passivation of Zn anode due to the accumulation of byproducts, which depends on the several factors such as testing rate, mass loading of cathodes, operating voltage, and inter-electrode distance.

According to the CV curves of ZICs at various rates (Figure S10), the rise at the upper potential vertex is sharper for lower rates (e.g., 5 mV/s) because there is more time for HER at the Zn anode for a lower scan rate. Therefore, there are likely more byproducts on the Zn anode surface when an ZIC is cycled at a lower rate, whereas there are limited side reactions for high-rate cycling. This implies that the failure mechanism of aqueous ZICs cycled at large current densities is likely a dendritic short circuit (rather than Zn passivation) provided that the inter-electrode distance is small. This agrees with a recent report that the Zn dendrites may ruin the batteries rapidly at large current densities and/or high loading mass of cathode materials in the neutral/mild electrolyte [10]. Thus, loosely assembled cells could explain the long life of aqueous ZICs cycled at high rates (10-20 A/g) which were reported in some studies [11-15].

The CV curves of the Org ZIC show a current rise near 2 V vertex at low rates (Figure S10d-e) is also an indication of the competitive HER during Zn deposition, which is because of the atmospheric uptake of water by the electrodes and Org electrolyte from the ambient as the assembly was carried out outside of an argon-filled glovebox.

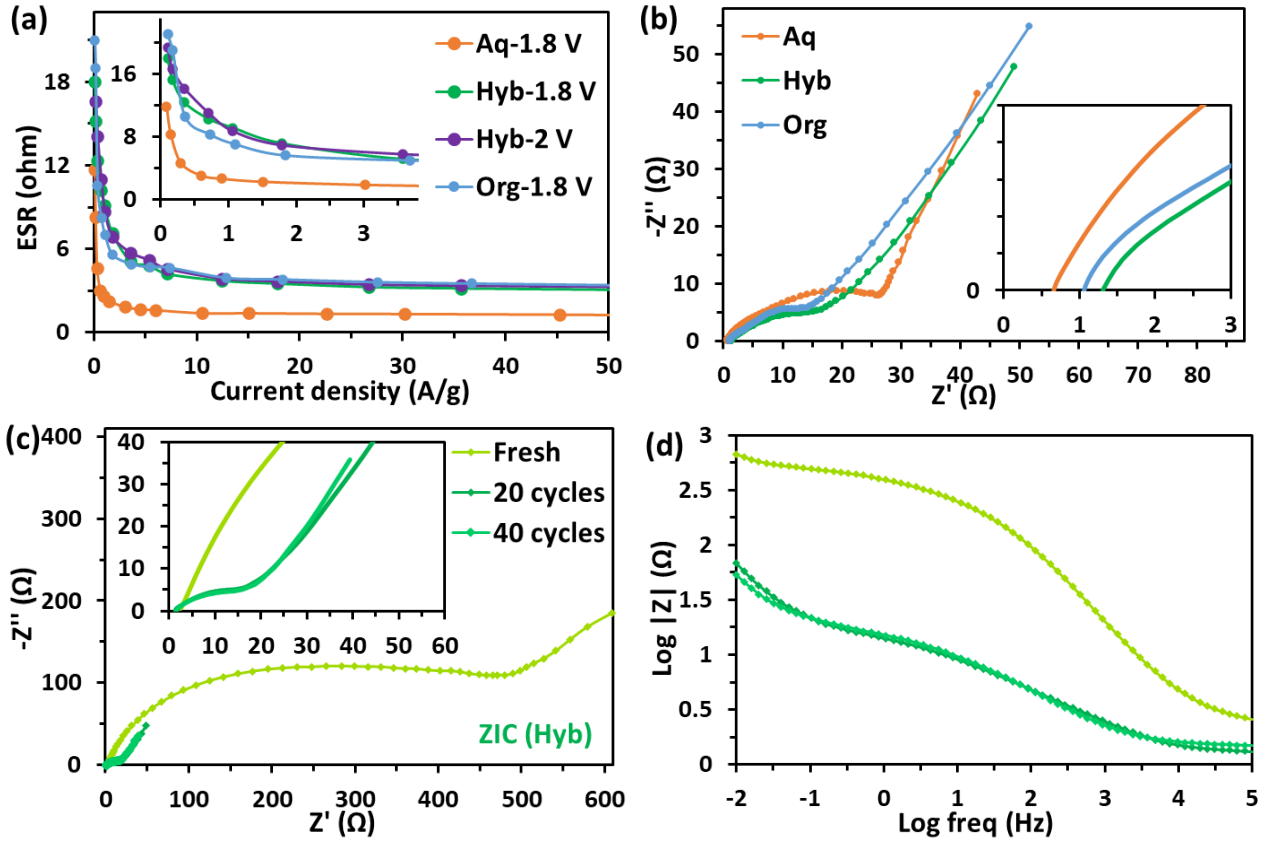

Figure S11. (a) ESR at various current densities obtained from GCD curves of ZICs with different electrolytes (see Figure 3a-c and Figure S9.). (b) Nyquist plots obtained from EIS tests of ZICs (EIS was conducted in the discharged state after 1-2h rest following 20-50 cycles of rate test). (c) Nyquist plot and (d) Bode impedance obtained from EIS tests of the Hyb ZIC. Figure S11c and d show that the impedance response of the freshly assembled ZIC is different from when it is cycled several times, which a common phenomenon for ZICs.

Table S4. Number of tests performed on aqueous ZICs before cell failure occurs. The accumulated number of rate tests were between 75-100, which included GCD tests (0.2-1.8 V, 0.3-150 mA), CV tests (0.2-1.8 V, 5-400 mV/s), and EIS. All aqueous ZICs failed during the charging stage, i.e., during Zn deposition on the Zn anode.

3M $Zn(OTf)_2$	No. of cycles	2M $ZnSO_4$	No. of cycles
Sample 1	63 (failed)	Sample 1	6 (failed)
Sample 2	36 (failed)	Sample 2	76 (failed)
Sample 3	45 (failed)	Sample 3	78 (failed)
Sample 4	55 (failed)	Sample 4	6 (failed)
Sample 5	38 (failed)	Sample 5	7 (failed)
Sample 6	100 (ok)	Sample 6	75 (ok)
Sample 7	100 (ok)	Sample 7	75 (ok)
Sample 8	15 (failed)		

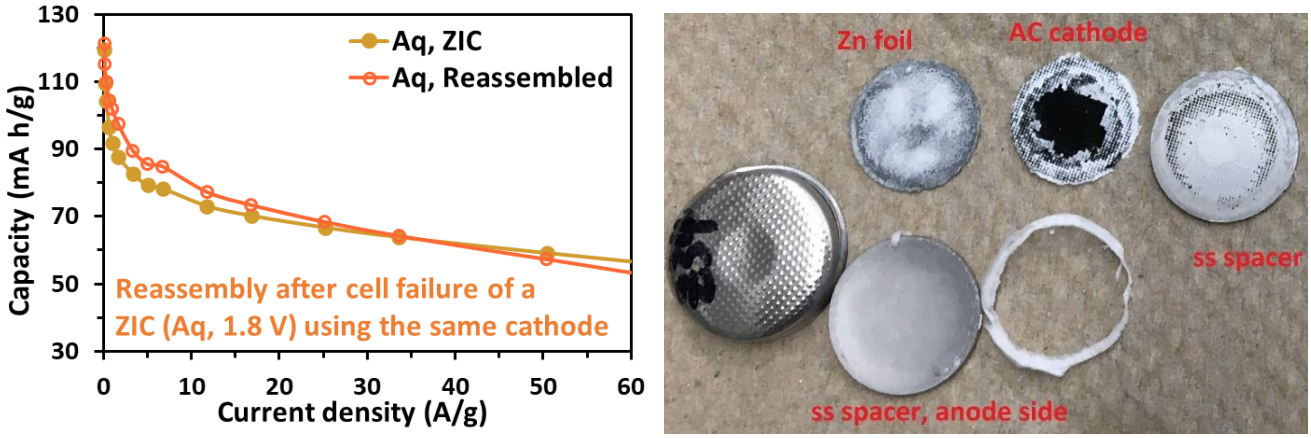

Figure S12. (a) Comparison of specific capacity of an Aq ZIC before and after reassembly. After the Aq ZIC died during the rate test (~ 45 cycles), the coin cell was opened and the AC cathode was retrieved. The same AC cathode but fresh electrolyte, separator, Zn foil, and coin cell components were used for the reassembly (new cell). The slight difference in the capacity could be because of a slight change in the density of the cathode as a result of experiencing compression during coin cell opening and reassembly. The mass loading of AC30 in the cathode is 2.35 mg/cm^2 (ZIC with 2M $ZnSO_4$). (b) The photo of the disassembled components of the Aq ZIC in (a) after cell failure, in which no yellowish color (iron rust) was observed.

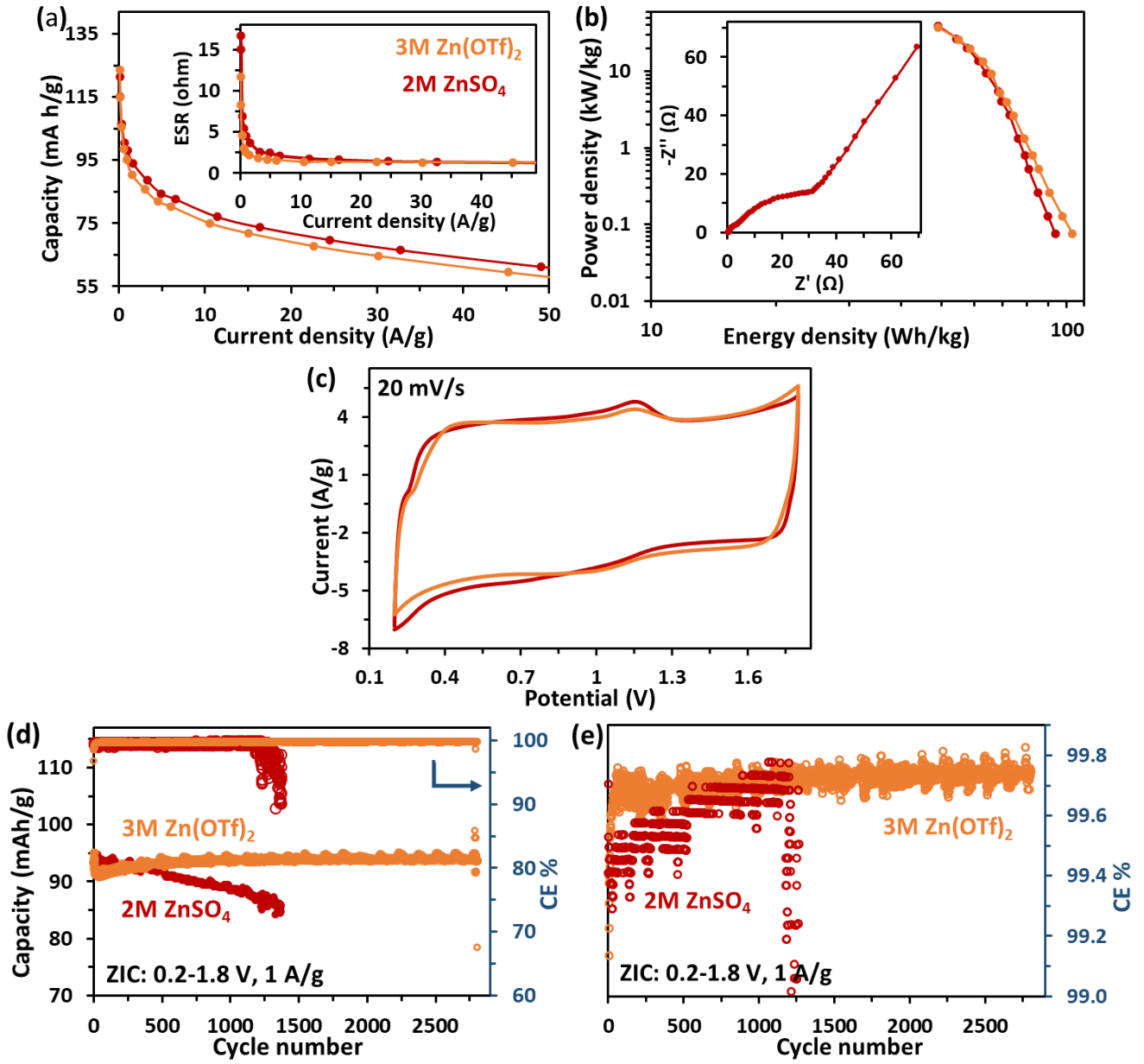

Figure S13. Electrochemical behavior of a ZIC assembled with 2M $ZnSO_4$ in comparison with the Aq ZIC; (a) Specific capacity and ESR (inset) at various current densities obtained from GCD curves of ZICs. (b) Ragone plots and Nyquist plot (inset). (c) CV curves of ZICs at 20 mV/s. (d) Cycling performance of ZICs within the voltage range of 0.2-1.8 V at 1 A/g. (e) The magnified CE of the ZICs shown in (d). The mass loading of AC30 in the cathode is 2.42 mg/cm^2 (ZIC with 2M $ZnSO_4$). The ZIC assembled with 2M $ZnSO_4$ showed similar capacitance and rate performance to that of Aq ZIC. However, it showed inferior cycle performance and lower CE than those of Aq ZIC.

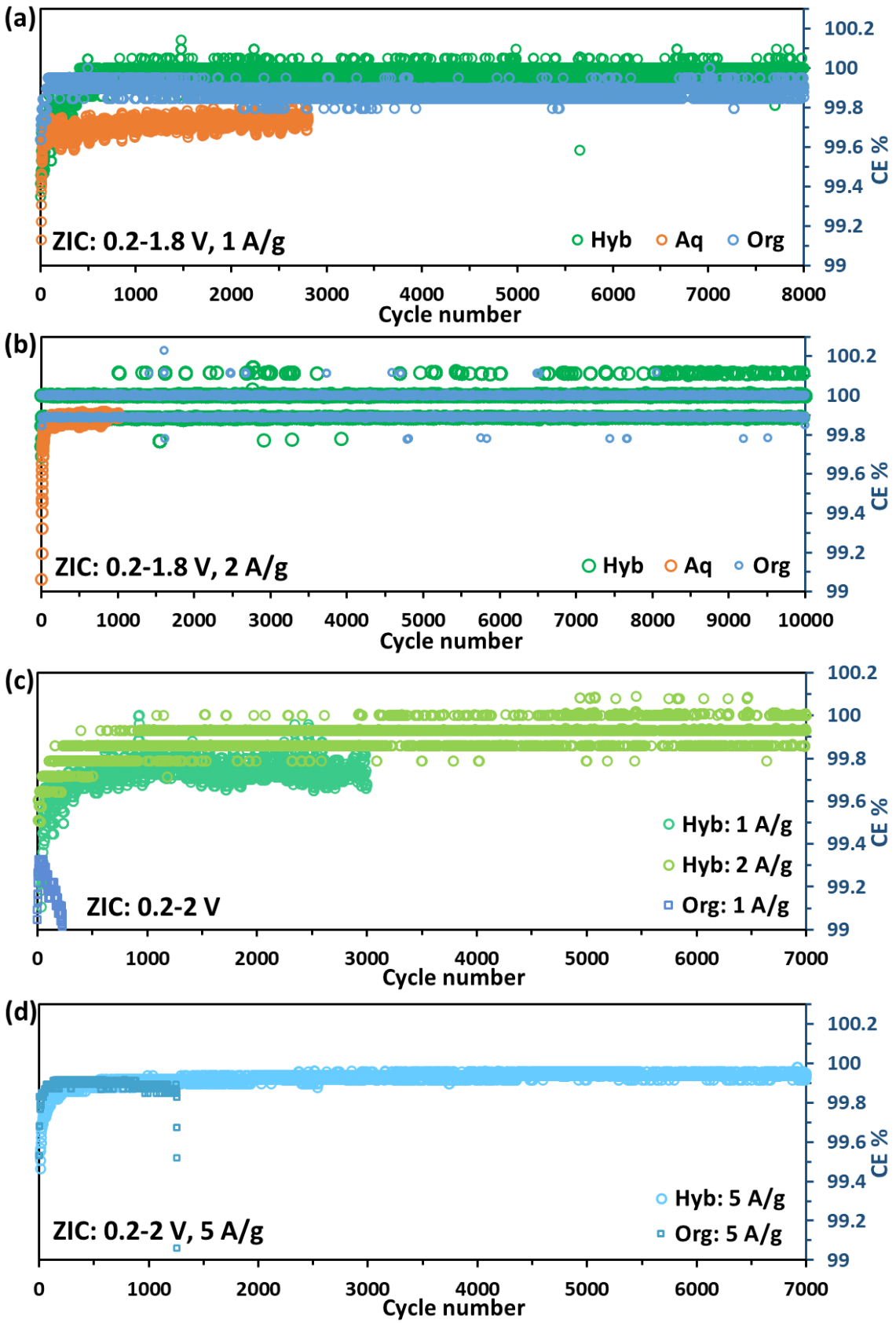

Figure S14. The magnified CE of ZICs shown in (a) Fig 3d, (b) Fig 3e, and (c, d) Fig 4c and Fig S40c.

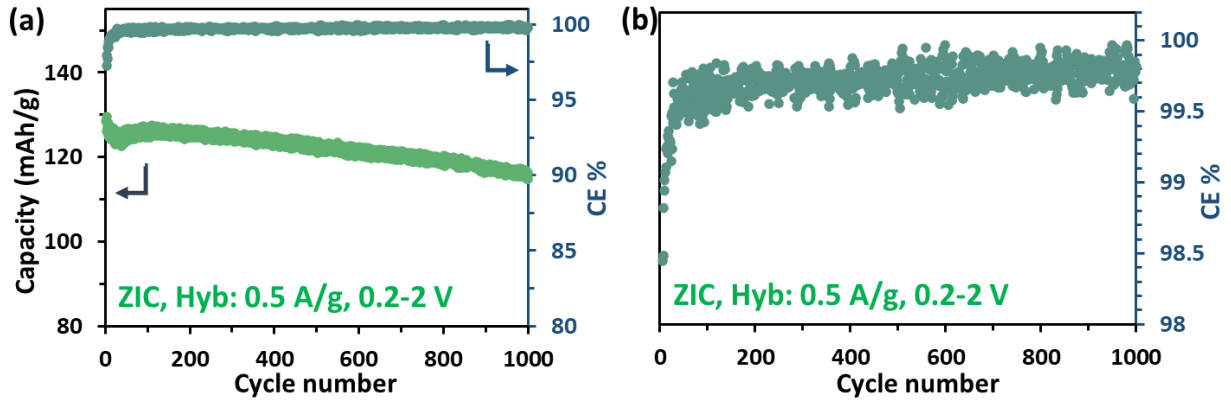

Figure S15. (a) Cycling performance of a Hyb ZIC in the range of 0.2-2 V at 0.5 A/g. (b) The magnified CE of the curve shown in (a).

Table S5. Summary of capacity retention and average CE of cycled ZICs.

Electrolyte, testing condition	Capacity retention% (cycles)	Avg. CE% (cycles)	AC30 loading (mg/cm^2)	Figure
2M $ZnSO_4$, 1.8 V, 1 A/g	90.9 (1,370)	99.69 (1,000)	2.42	Figure S13d
Aq, 1.8 V, 1 A/g	96.4 (2,800)	99.76 (2,800)	3.39	Figure 3d, Figure S14a
Hyb, 1.8 V, 1 A/g	98.5 (8,000)	99.96 (8,000)	2.15	Figure 3d, Figure S14a
Org, 1.8 V, 1 A/g	99.9 (8,000)	99.88 (8,000)	2.49	Figure 3d, Figure S14a
Aq, 1.8 V, 2 A/g	99.3 (1,014)	99.87 (1,000)	3.91	Figure 3e, Figure S14b
Hyb, 1.8 V, 2 A/g	99.2 (10,000)	99.97 (10,000)	2.46	Figure 3e, Figure S14b
Org, 1.8 V, 2 A/g	102.4 (10,000)	99.95 (10,000)	2.69	Figure 3e, Figure S14b
Hyb, 2 V, 0.5 A/g	91.7 (1,000)	99.71 (1,000)	3.21	Figure S15
Hyb, 2 V, 1 A/g	83.0 (3,000)	99.72 (3,000)	2.10	Figure 4c, Figure S14c
Hyb, 2 V, 2 A/g	87.1 (7,000)	99.90 (7,000)	2.02	Figure 4c, Figure S14c
Hyb, 2 V, 5 A/g	90.3 (7,000)	99.92 (7,000)	2.22	Figure 4c, Figure S14d
Org, 2 V, 1 A/g	100.6 (230)	99.20 (230)	2.22	Figure S14c, Figure S40c-d
Org, 2 V, 5 A/g	97.9 (1262)	99.88 (1262)	2.15	Figure S14d, Figure S40c-d

ZIC vs supercapacitor with the Hyb electrolyte:

To highlight the advantage of ZICs over symmetric SCs, the Hyb ZIC was compared with a Hyb SC in which both electrodes have identical area and loading of AC30 to that the ZIC (2.22 mg/cm^2). According to Figure S16, the Hyb ZIC shows superior capacity and energy density than those of the Hyb SC when they are tested up to 1.8 V and 2 V. In other words, switching one AC-based electrode of a SC with a Zn foil leads to elevated storage capability without a loss in rate performance. The ZIC can function at a lower rate than the SC with significant gains in capacity and energy, while the SC yields low CE for currents lower than 5 mA. Moreover, the capacity (and thus capacitance) of the SC is unchanged when the cell voltage is increased from 1.8 V to 2 V, as expected in SCs. In contrast, a significant increase in the capacity and energy density of the Hyb ZIC is observed when its upper-limit voltage extends from 1.8 V to 2 V, which proves the role of the Zn anode in the voltage-dependent storage of Hyb ZICs.

Figure S16c shows the cycling stability of the Hyb SC in the voltage range of 0-2 V, which indicates that the Hyb electrolyte is stable regardless of the role of Zn anode. The Hyb SC maintained 83.0% of its capacitance with an average CE of 99.92% after 10,000 cycles of GCD at 11.7 mA/cm^2. When cycled at 23.5 mA/cm^2, this SC showed a capacitance retention of 102.3% with a CE of 100% after 20,000 cycles. Thus, this Hyb SC experiences a faster capacitance decay when it is cycled at a lower rate, just like the Hyb ZIC working up to 2 V (Figure 4c). This suggests that the capacity degradation of the Hyb ZIC cycled at 2 V and lower rates originates from the Hyb electrolyte rather than passivation or corrosion of the Zn surface.

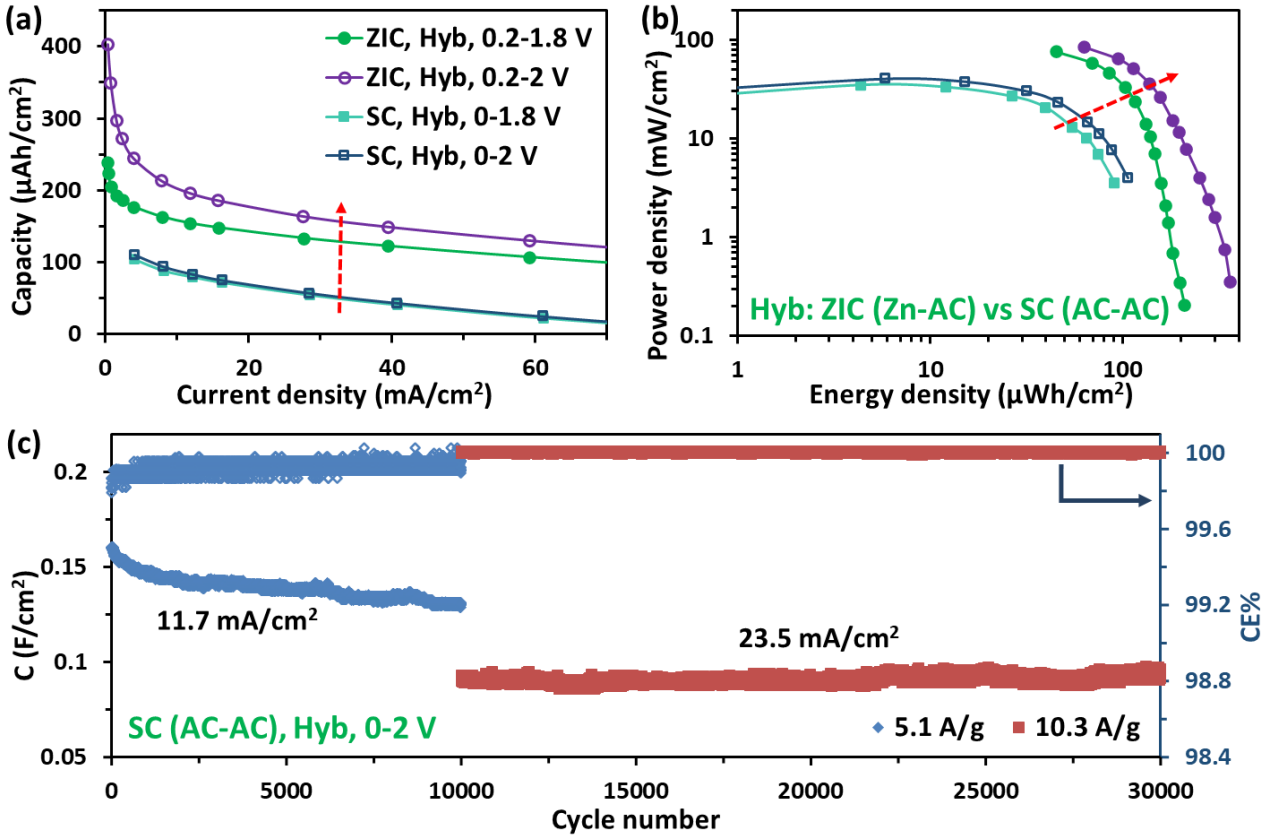

Figure S16. Comparison of the electrochemical behavior of the Hyb ZIC and the Hyb supercapacitor (SC). (a) Areal specific capacity various current densities obtained from GCD curves. (b) Areal Ragone plots. (c) Cycling performance of Hyb SC in the range of 0.2-2 V. The SC was assembled with 80 µl of the Hyb electrolyte. The mass loading of activated carbon (AC30) is 2.22 mg/cm^2 for the ZIC cathode as well as both electrodes of the SC.

Tuning the molar ratio of AN to water in the hybrid electrolyte:

The molar ratio of AN to water was tuned based on the rate performance of 1.8 V ZICs. By maintaining the salt concentration to the saturated level, three hybrid electrolytes were prepared with different AN/water molar ratios of 1, 1.53, 0.75 (or salt/H_2O/AN molar ratio of 1:3.5:3.5, 1:3:4.6, and 1:4:3). This was done by fixing one ratio and finding the other co-solvent ratio to get a saturated solution (e.g., fixing water/salt ratio of 3 and find the ratio of AN/salt).

All three ZICs fabricated from three hybrid electrolytes show similar capacity at low rates while the Hyb ZIC (1:3.5:3.5) has the best rate performance (Figure S17a). The comparison of the CV curves for 5 and 50 mV/s also reveals that the equal molar ratio of AN to water yields the best rate capability. The difference in the performance of these electrolytes could be originated from the solvation structure that defines the ionic conductivity and diffusion behavior.

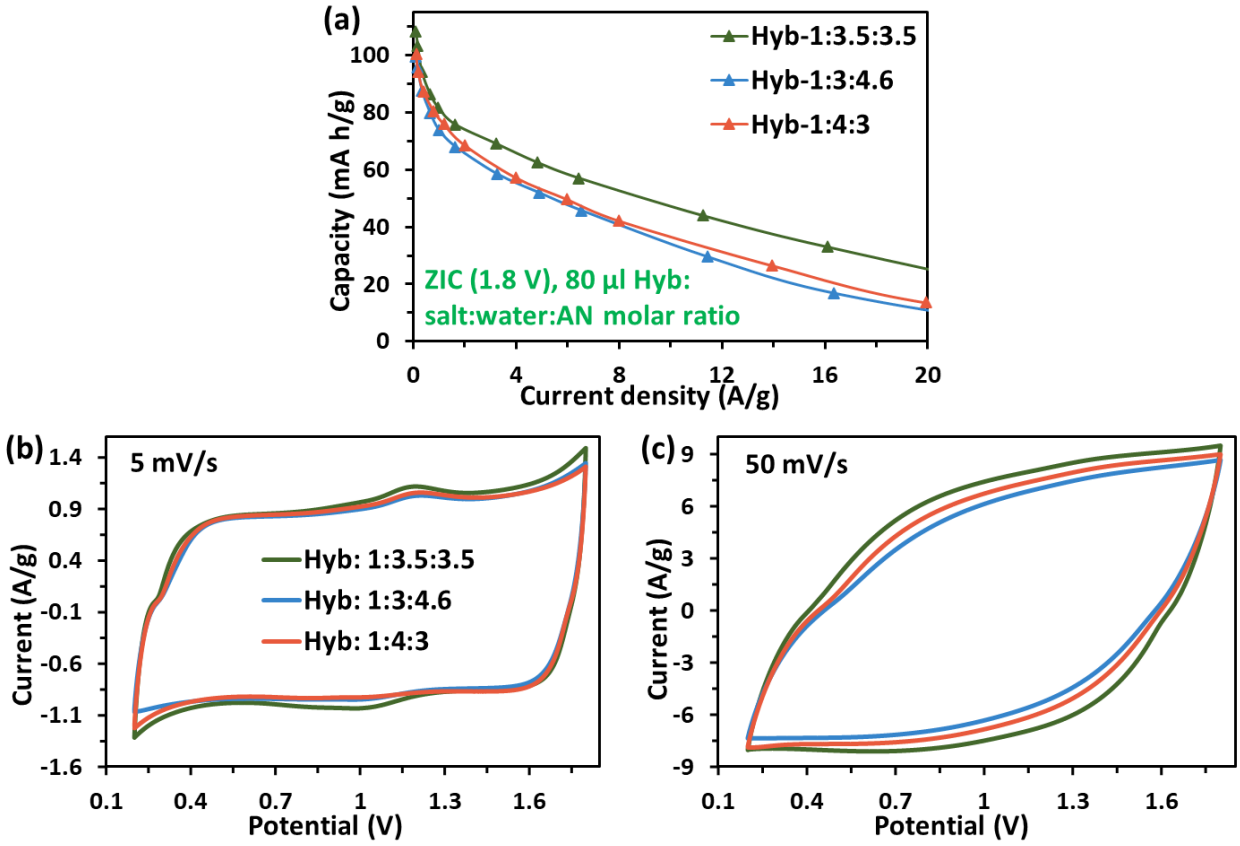

Figure S17. Electrochemical behavior of ZICs in different hybrid electrolytes with different ratio of AN and water (saturated electrolytes with salt/H_2O/AN molar ratio of 1:3.5:3.5, 1:3:4.6, and 1:4:3); (a) Specific capacity of ZICs at various current densities within the voltage range of 0.2-1.8 V, and (b) CV curves of ZICs at 5 and 50 mV/s. The mass loading of AC30 in the cathodes are 3.10 mg/cm^2 (1:3.5:3.5), 3.06 mg/cm^2 (1:3:4.6), and 2.51 mg/cm^2 (1:4:3).

Effect of electrolyte amount on the performance of Hyb ZICs:

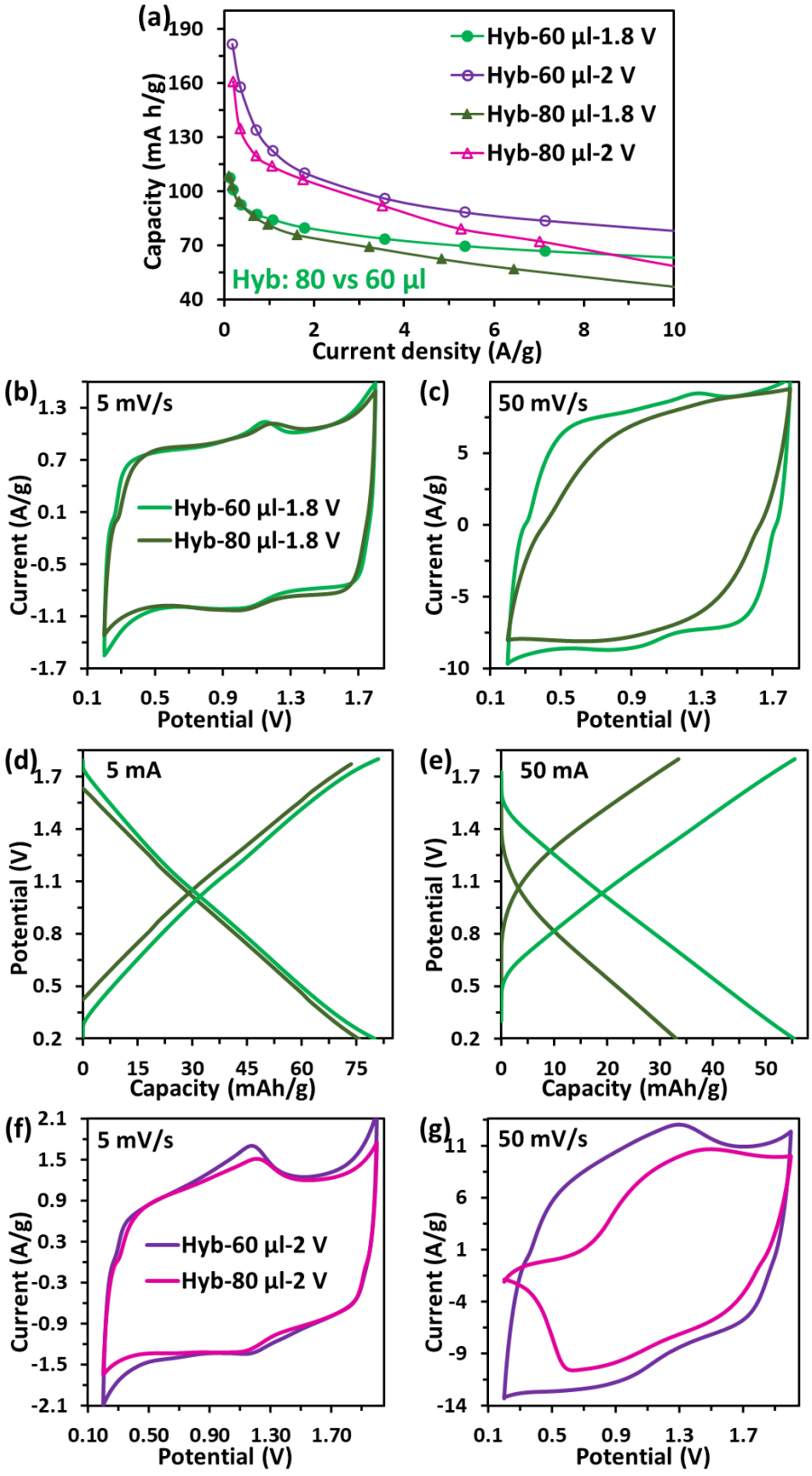

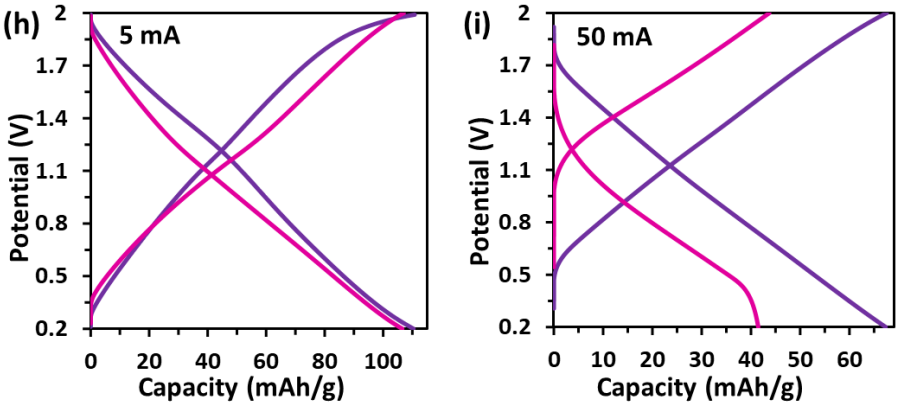

Figure S18. The effect of electrolyte amount on performance of Hyb ZICs. (a) Comparison of specific capacity for Hyb ZICs assembled with 60 µl and 80 µl of electrolyte within the voltage range of 0.2-1.8 V and 0.2-2 V. (b-e) CV and GCD curves of ZICs for low and high rates in the range of 0.2-1.8 V. (f-i) CV and GCD curves of ZICs for low and high rates in the range of 0.2-2 V. The mass loading of AC30 in the cathodes are 2.22 mg/cm^2 (60 µl), 3.10 mg/cm^2 (80 µl, 1.8 V), 2.85 mg/cm^2 (80 µl, 2 V).

In this work, the amount of the Hyb electrolyte was tuned based on the capacitive performance. The results show that the amount of electrolyte may have a substantial impact on the capacitive performance of Hyb ZICs. For example, the Hyb ZIC with 60 µl of electrolyte showed better capacity and rate performance than the cell with 80 µl Hyb electrolyte for both 1.8 and 2 V cells (Figure S18). This value is valid for the setup used herein, i.e., CR2032 coin cells, glass fiber separator, 2 spacers, and AC30 loading of 2-4 mg/cm^2 (see experimental section).

The comparison of GCD and CV curves of ZICs for low and high rates in the range of 0.2-1.8 V reveals that the cell with 60 µl Hyb electrolyte has lower equivalent resistance (thus better rate capability) than the one with 80 µl (Figure S18b-e). This is reflected in its lower potential drop in the GCD curve at 50 mA and less oblique CV curves at 50 mV/s. The higher resistance of the ZIC with 80 µl could be due to the adverse effect of the AN-containing Hyb electrolyte on the conductivity of the AC30-based cathode when it is wetted with more electrolyte than required.

Aside from conductivity challenge, a common issue in hybrid capacitors is the kinetic imbalance between the battery-type anode and the capacitor-type cathode [16]. The storage mechanism of ZICs mainly involves Zn plating/stripping at the anode surface and the adsorption/desorption of anions in and out of the cathode. The potential windows of the anode (V_{anode}) and the cathode ($V_{cathode}$) increase with increasing the cell voltage (Figure S19), but the increased contribution of each electrode depends on the various factors such as the nature of electrodes (e.g., mass [16], state of charge [17]) and electrolyte.

When the upper-limit voltage of a Hyb ZIC extends from 1.8 V to 2 V, the elevated potential window of the anode (V_{anode}) may be unfavorable for the Zn anode because of its rate-dependent Faradic nature not performing well at high rates (unlike the cathode). It appears that such potential change of the anode can be manipulated by the amount of the Hyb electrolyte. For instance, for the Hyb ZIC with 80

µl of electrolyte tested in the range of 0.2-2 V, the unfavorable potential range of Zn anode (larger rise in V_{anode}) is reflected in the distorted GCD and CV curves at high rates around the lower voltage bound (Figure S18f-i). Thus, this shifts the effective lower bound of the cell voltage to higher values (limited discharge around 0.2 V). Since the capacitor-type cathode performs well at a high rate, this issue has to do with the anode side. This poor rate performance at 2 V cannot be fully explained by the conductivity difference that was observed for 1.8 V ZICs. In contrast, the cell with 60 µl of electrolyte is more tolerant to this "potential range imbalance" when operating in the range of 0.2-2 V. Hence, tuning the volume of Hyb electrolyte is essential when ZICs are operating in the extended voltage. Nevertheless, fundamental understanding of the mechanism can be realized by monitoring the potential variation of anode and cathode by introducing independent reference electrodes, which remains for future work.

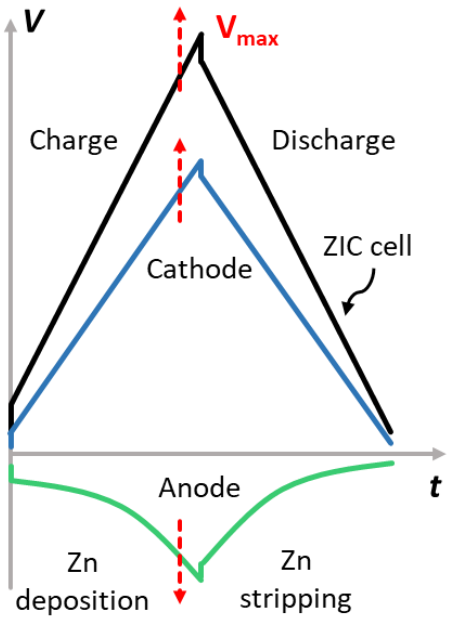

Figure S19. Schematic depiction of charge-discharge curve for a ZIC (Zn anode and activated carbon cathode). The blue and green curves are charge-discharge curves of the cathode and anode with respect to a reference electrode with arbitrary values (unreal) shown for the sake of demonstration. The cell voltage is the difference between the potential window of the cathode and anode ($V_{cell} = V_{cathode} - V_{anode}$) at any time during the charge or discharge. The red arrows show that the contributions of Zn anode (V_{anode}) and the cathode ($V_{cathode}$) increase upon increasing the cell voltage. The contribution of each electrode usually depends on the nature of each electrode and the electrolyte, which can be defined using reference electrodes.

Table S6. Summary of typical parameters of ZICs (two-electrode cell) from other studies (Figure 4a, b).

Reference	Electrodes: anode// cathode	Electrolyte, voltage range	Cathode loading* (mg/cm^2)	Max capacity* mAh/g	Max energy density* Wh/Kg
This work	Zn//AC30	**Hyb**: $Zn(CF_3SO_3)_2$/ $(H_2O)_{3.5}$/$(AN)_{3.5}$, **0.2-2 V**	2.22	181.6 (0.18 A/g)	162.1
This work		**Hyb**, **0.2-1.8 V**	2.22	107.9 (0.11 A/g)	94.1
This work (control)		**Aq**: 3M $Zn(CF_3SO_3)_2$, **0.2-1.8 V**	2.62	123.7 (0.09 A/g)	103.1
This work (control)		**Org**: 1M $Zn(CF_3SO_3)_2$ in AN, **0.2-1.8 V & 2 V**	2.15	86.7 (0.18 A/g)	78.8
Ref A [18] (Energy Storage Mater. 2018, 13, 96)	Zn//AC	Aqueous: 2M $ZnSO_4$, **0.2-1.8 V**	0.7-0.8 (mg/cm^2)	121 (0.1 A/g)	84
Ref B [19] (Electrochim. Acta 2019, 327, 134999)	Zn//HPC	Aqueous: 2M $ZnSO_4$, **0.01-1.8 V**	0.9 (mg/cm^2)	204 (0.2 A/g)	97.9
Ref C [12] (Adv. Energy Mater. 2019, 9, 1902915)	Zn//aMEGO	Aqueous: 3M $Zn(CF_3SO_3)_2$, **0-1.9 V**	NA	~106 (0.1 A/g)	~101
Ref D [20] (Nano Energy 2019, 66, 104132)	Zn//LDC	Aqueous: 1M $ZnSO_4$, **0.2-1.8 V**	~2 (mg/cm^2)	127.7 (0.5 A/g)	97.6
Ref E [21] (Joule 2019, 3, 1289)	Zn//AC; Zn@MOF//AC	Aqueous: 2M $ZnSO_4$, **0.2-1.8 V**	6 (mg/cm^2)	132 (0.1 A/g)	106.1
Ref F [22] (Adv. Energy Mater. 2020, 10, 2001705)	Zn//PC; Zn@PC//PC	Aqueous: 3M $Zn(ClO_4)_2$, **0-1.9 V**	1.4-2 (mg/cm^2)	179.8 (0.1 A/g)	104.8
Ref G [23] (Energy Storage Mater. 2018, 13, 1)	Zn//AC	Organic: 1M $Zn(CF_3SO_3)_2$ in AN, **0-1.8 V**	NA	84.1 (0.1 A/g)	61.6
Ref H [24] (J. Mater. Chem. A 2019, 7, 7784)	Zn@carbon cloth//HCS	PAM-$ZnSO_4$ gel, **0.15-1.95 V**	1-1.2 (mg/cm^2)	86.8 (0.5 A/g)	59.7

Ref I [25] (Energy Environ. Sci. 2020, 13, 3527)	Zn//N-doped AC	Hybrid: 2M $ZnSO_4/H_2O$/EG (40 vol%), **0.2-1.8 V**	2.5-3 (mg/cm^2)	98.7 (0.1 A/g)	82.0

* Mass loading, capacity, and energy density were calculated based on the mass of active materials in the cathode for all the references. AC (commercial activated carbons), HPC[19] (hierarchical porous carbon), aMEGO[12] (activated graphene), LDC[20] (2D layer porous carbon), MOF[21] (metal organic framework, Zn@ZIF-8-500), PC[22] (oxygen-rich porous carbon), HCS[24] (hollow carbon spheres), and PAM [24] (polyacrylamide).

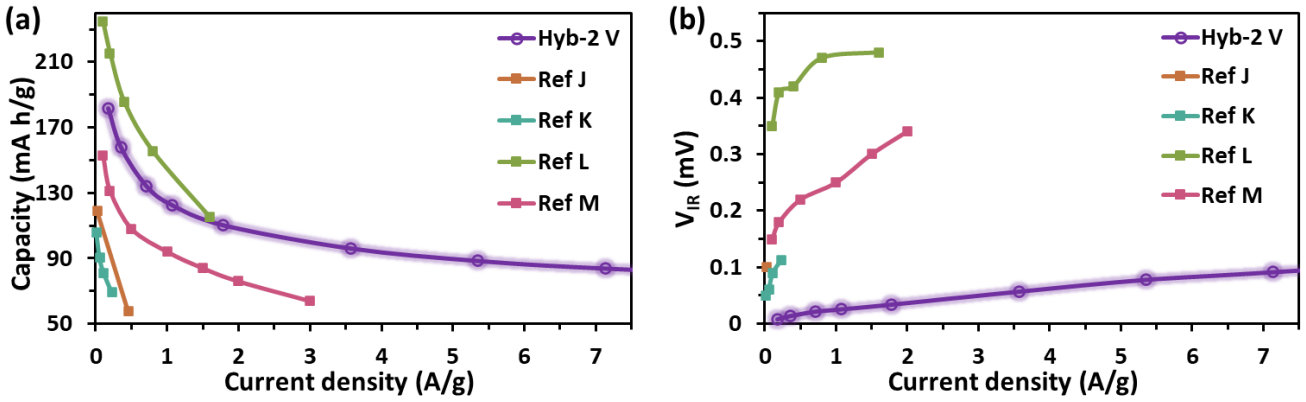

Figure S20. Performance comparison of the Hyb ZIC (this work) with ZIBs assembled with super-concentrated electrolytes reported in the literature (Ref J [26], Ref K [27], Ref L [28], Ref M [29]; see Table S7 for details of electrodes and electrolytes); (a) capacity (based on active materials in the cathode) and (b) potential drop at the beginning of the discharge curve (V_{IR}).

Table S7. Summary of typical parameters of ZIBs with super-concentrated electrolytes from other studies (Figure S20).

Reference	Electrodes: anode/ cathode (mg/cm^2)	Electrolyte	Capacity mAh/g (rate); (voltage range)	Capacity retention%, cycles (A/g); CE%
This work	Zn//AC30 (2.22)	Hyb (4.8 m): $Zn(CF_3SO_3)_2$/ $(H_2O)_{3.5}$/$(AN)_{3.5}$	181.6 (0.18 A/g); 83.8 (7.13 A/g); (0.2-2V)	83.0%, 3k (1 A/g); 87.1%, 7k (2 A/g); 90.3%, 7k (5 A/g); avg CE: >99.7
Ref J [26] (Nat. Mater. 2018, 17, 543)	Zn//$LiMn_2O_4$ (NA)	Water-in-bisalt: 1 m $Zn(TFSI)_2$ + 20 m LiTFSI	118.8 (0.023 A/g); (0.8-2.1 V)	83.8%, 500 (0.023 A/g); 85.0%, 4k (0.46 A/g); CE: ~99.6-100.1%
Ref K [27] (Nano Energy 2019, 57, 625)	Zn//$LiMn_2O_4$ (5)	Water-in-deep eutectic solvent: LiTFSI/$Zn(TFSI)_2$/ Urea/H_2O, molar ratio (1:0.05:3.8:2)	106 (0.012 A/g); 69 (0.23 A/g); (1.5-2.2 V)	90.8%, 300 (0.012 A/g); 82.7%, 600 (0.058 A/g); 86.6%, 600 (0.23 A/g); CE: ~98-100%
Ref L [28] (Energy Storage Mater. 2020, 28, 205)	Zn//MnO_2 (1)	Water-in-bisalt: 1 m $Zn(OAc)_2$ + 31 m KOAc	237.6 (0.1 A/g); 117.3 (1.6 A/g); (0.8-2 V)	79.7%, 600 (0.1 A/g); CE: ~98-99.9%
Ref M [29] (Adv. Funct. Mater. 2020, 30, 2003511)	Zn//$Na_3V_2(PO_4)_2O_{1.6}F_{1.4}$ (1)	Water-in-bisalt: 25 m $ZnCl_2$ + 5 m NH_4Cl	153 (0.1 A/g); 64 (3 A/g); (0.4-2.1 V)	82.7%, 2k (0.5 A/g); 73.5%, 7k (2 A/g); CE: ~99-99.7%
[30] (Adv. Funct. Mater. 2019, 29, 1902653)	Zn//$Ca_{0.2}V_2O_5$ (3-4)	Water-in-salt: 30 m $ZnCl_2$	248 (0.05 A/g, three-electrode system); (0.2-1.8 V)	51.1%, 100 (0.05 A/g); 70.0%, 1000 (1.6 A/g); CE: ~98-100%
[31] (Chem. Commun., 2021, 57, 1246)	Zn/MnO_2 (0.9)	Super-saturated hybrid (16.8 m): $Zn(CF_3SO_3)_2$/ $(H_2O)_{1.85}$/$(AN)_{0.64}$	215 (0.03 A/g); (0.8-2 V)	53.5%, 200 (2 V, 0.03 A/g); 47.3%, 200 (2.2 V, 0.03 A/g)

- For $LiMn_2O_4$, the capacity at 1 C is assumed 115 mAh/g (i.e., 1 C is 0.115 A/g).

- All the capacity values are based on the mass of active materials in the cathode.

- CE% was not verified in most references due to the wide range of data presentation (i.e., 0-100%).

- We used the term "super-saturated" to describe the electrolyte in Ref [31] because its concentration (i.e., 16.8 mol kg^{-1} calculated from reported data) is significantly beyond the solubility threshold of $Zn(CF_3SO_3)_2$ (less than 5 mol kg^{-1}) at room temperature.

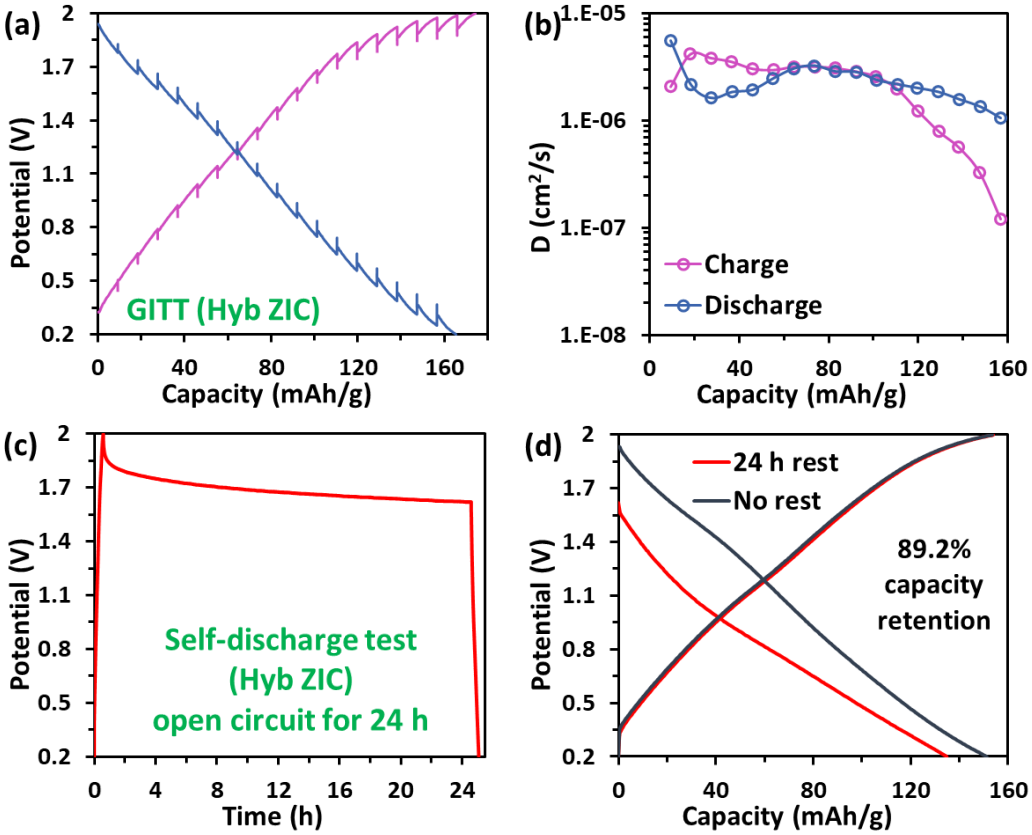

Figure S21. (a) Charge-discharge GITT profile of the Hyb ZIC (11th cycle) and (b) the corresponding diffusion coefficients. (c-d) Self-discharge behavior of the Hyb ZIC after resting 24 h (15th cycle no rest and 16th cycle 24 h rest). Both the GITT and self-discharge tests were carried out in the voltage range of 0.2-2 V at the current of 1 mA. The mass loading of AC30 in the cathode used in this Hyb ZIC is 3.2 mg/cm^2 (electrode diameter: 1.2 cm).

The GITT test was conducted by applying a constant current for 2 min alternated with 10 min OCV periods. The diffusion coefficient was calculated using $D = (4L^2/\pi t)(\Delta E_s/\Delta E_t)^2$, where L (cm) is the ion diffusion length (it is electrode thickness for compact electrode), t (s) is the duration of the current pulse, ΔE_s (V) is the steady-state potential change (the difference in the OCV measured at the end of the rest period of two successive steps), ΔE_t (V) is the potential change during the current pulse minus the iR drop [32].

Effect of working voltage on the cycle performance ZICs:

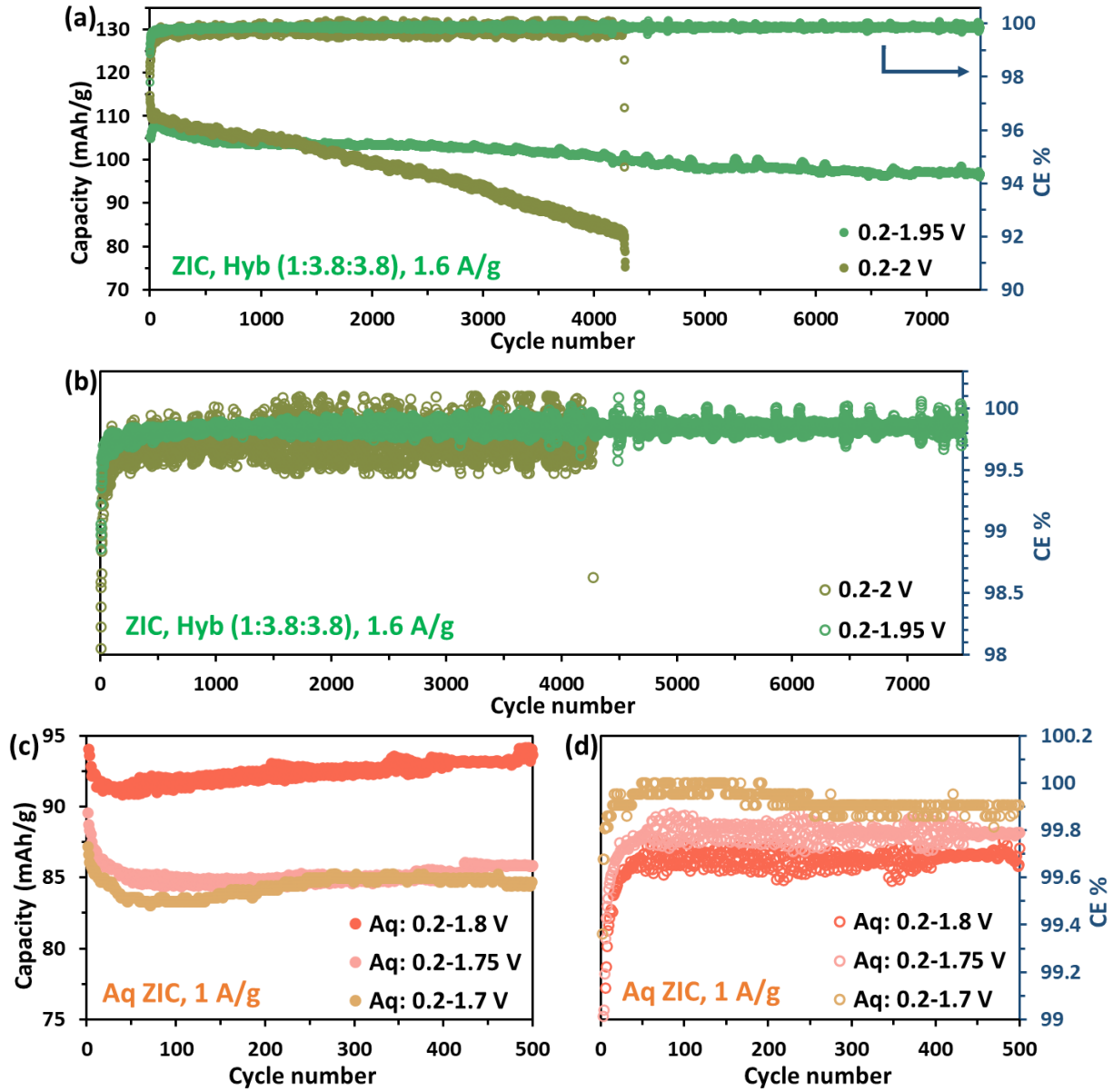

Figure S22. (a) The cycle performance of ZICs assembled using a more dilute hybrid electrolyte with a molar ratio of 1:3.8:3.8, and (b) the magnified CE. The cells were tested at 1.6 A/g in the range of 0.2-1.95 V (2.62 mg/cm^2) and 0.2-2 V (2.59 mg/cm^2). The diluted hybrid electrolyte (1:3.8:3.8) has inferior stability than the Hyb (1:3.5:3.5) when it is cycled at 2 V. This diluted hybrid electrolyte shows a better capacity retention and CE when cycled up to 1.95 V, indicating that 1.95 V is the stability threshold for this electrolyte. (c) Comparison of the cycle performance of Aq ZICs for 500 cycles in the voltage range of 0.2-1.8 V (3.39 mg/cm^2), 0.2-1.75 V (3.39 mg/cm^2), and 0.2-1.7 V (2.62 mg/cm^2), and (d) the magnified CE. With increasing the working voltage of the Aq ZIC, the capacity increases. However, increasing the working voltage of the Aq ZIC leads to inferior CE due to increased HER.

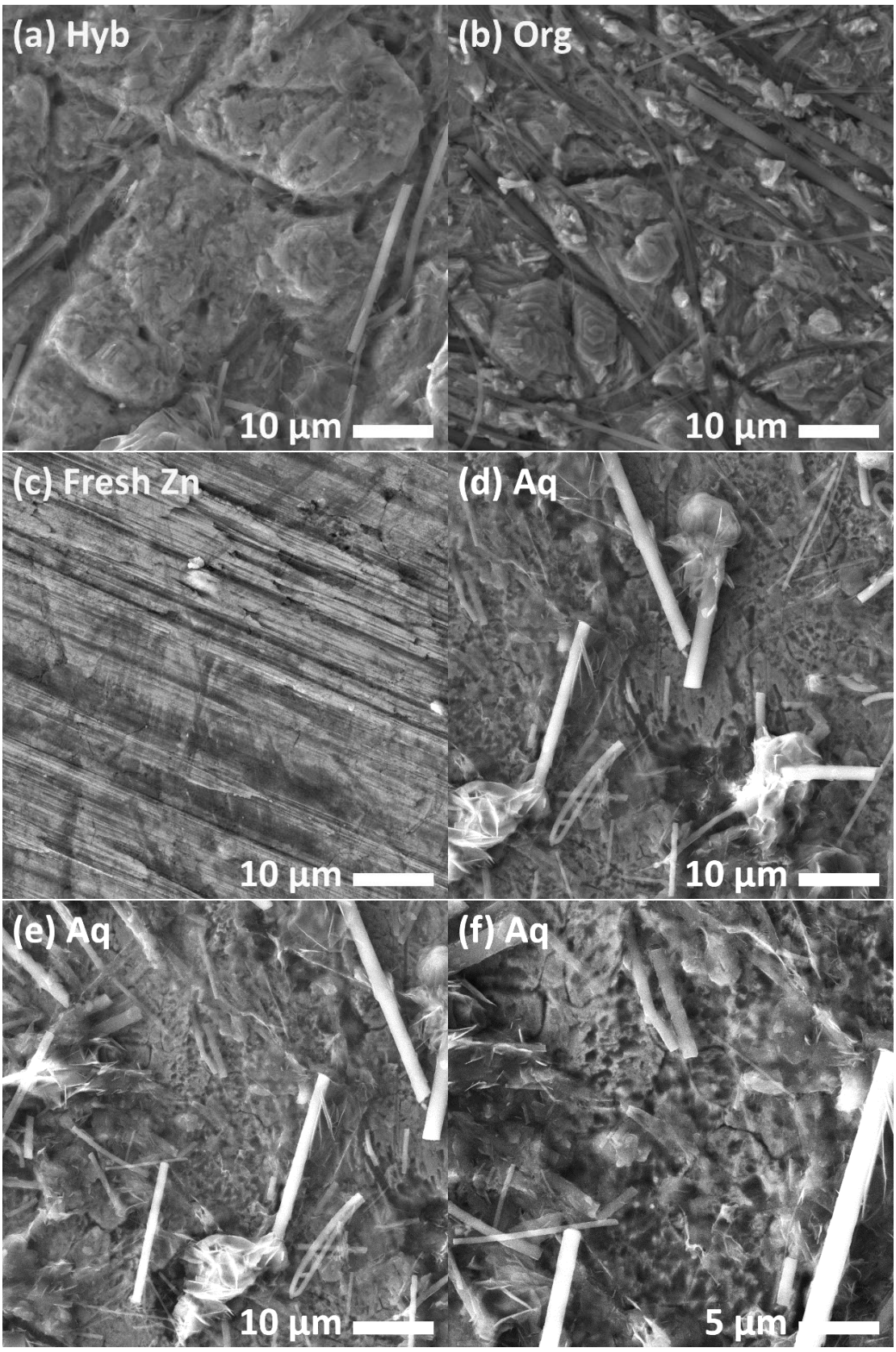
(a) Hyb
10 µm
(b) Org
10 µm
(c) Fresh Zn
10 µm
(d) Aq
10 µm
(e) Aq
10 µm
(f) Aq
5 µm

Figure S23. Additional higher-magnification SEM images of post-cycled Zn foils presented in Fig 4: (a) Hyb (3,000 cycles, 1 A/g, 0.2-2 V), (b) Org (232 cycles, 1 A/g, 0.2-2 V), (c) fresh Zn foil,(d-f) Aq (63 cycles of rate test, 0.2-1.8 V). The rod-shaped microfibers are the residue of glass microfiber separators remained on the Zn foils after cycling.

Table S8. Summary of EDS elemental compositions of posit-cycled Zn foils obtained from ZICs (Figure S24-26, S28). Zn foils were extracted from ZICs after undergoing GCD cycles: Hyb (3,000 cycles, 1 A/g, 0.2-2 V), Org (232 cycles, 1 A/g, 0.2-2 V), and Aq (63 cycles of rate test, 0.2-1.8 V).

Cycled Zn foils	Zn Wt%	O Wt%	C Wt%*	Wt% of other elements
Zn fresh (Figure S24)	92.5	1.0	6.5	-
Hyb, site 1 (Figure S25a)	90.3	3.3	5.2	F 0.7; S 0.3
Hyb, site 2 (Figure S25b)	85.3	6.0	7.3	F 0.8; S 0.3
Hyb, site 3 (Figure S25c)	85.5	6.1	6.3	F 1.3; S 0.5
Org, site 1 (Figure S26a)	86.2	6.4	6.4	F 0.5; S 0.2
Org, site 2 (Figure S26b)	86.6	7.3	5.6	Si 0.6
Org, site 3 (Figure S26c)	78.9	10.8	5.2	S 0.5; Si 3.9
Aq, site 1 (Figure S28a)	82.8	9.8	7.1	-
Aq, site 2 (Figure S28b)	76.2	15.5	7.1	Si 1.3
Aq, site 3 (Figure S28c)	46.1	23.9	4.4	F 16.6; S 7.8; Si 1.4

* 4-7 Wt% of carbon on the surface of Zn foils is due to carbon contaminations (typically C-C, C-O-C, and O-C=O components), which is also seen on the surface of fresh Zn.

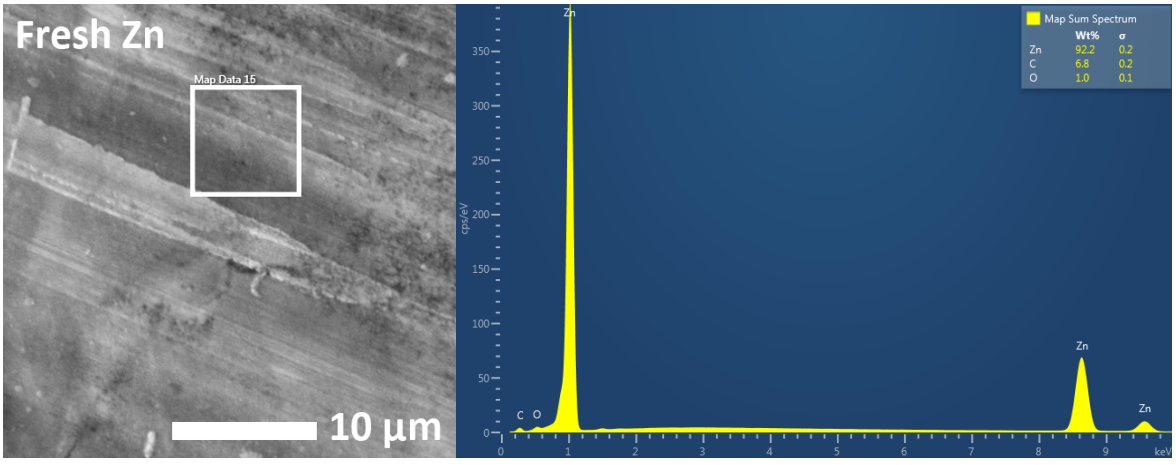

Figure S24. EDS image of fresh Zn foil.

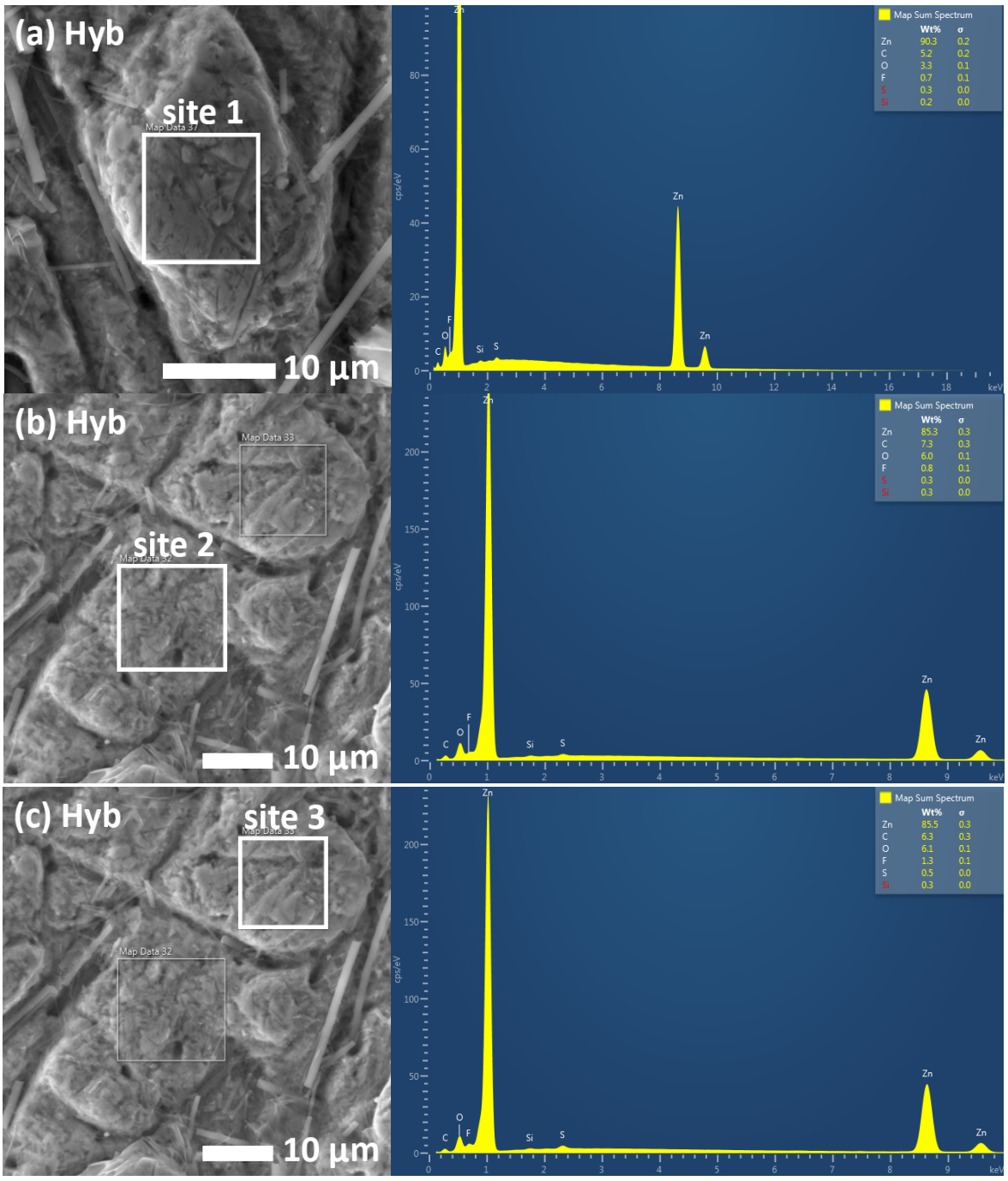

Figure S25. EDS images of Zn foil obtained from a Hyb ZIC (3,000 cycles, 1 A/g, 0.2-2 V).

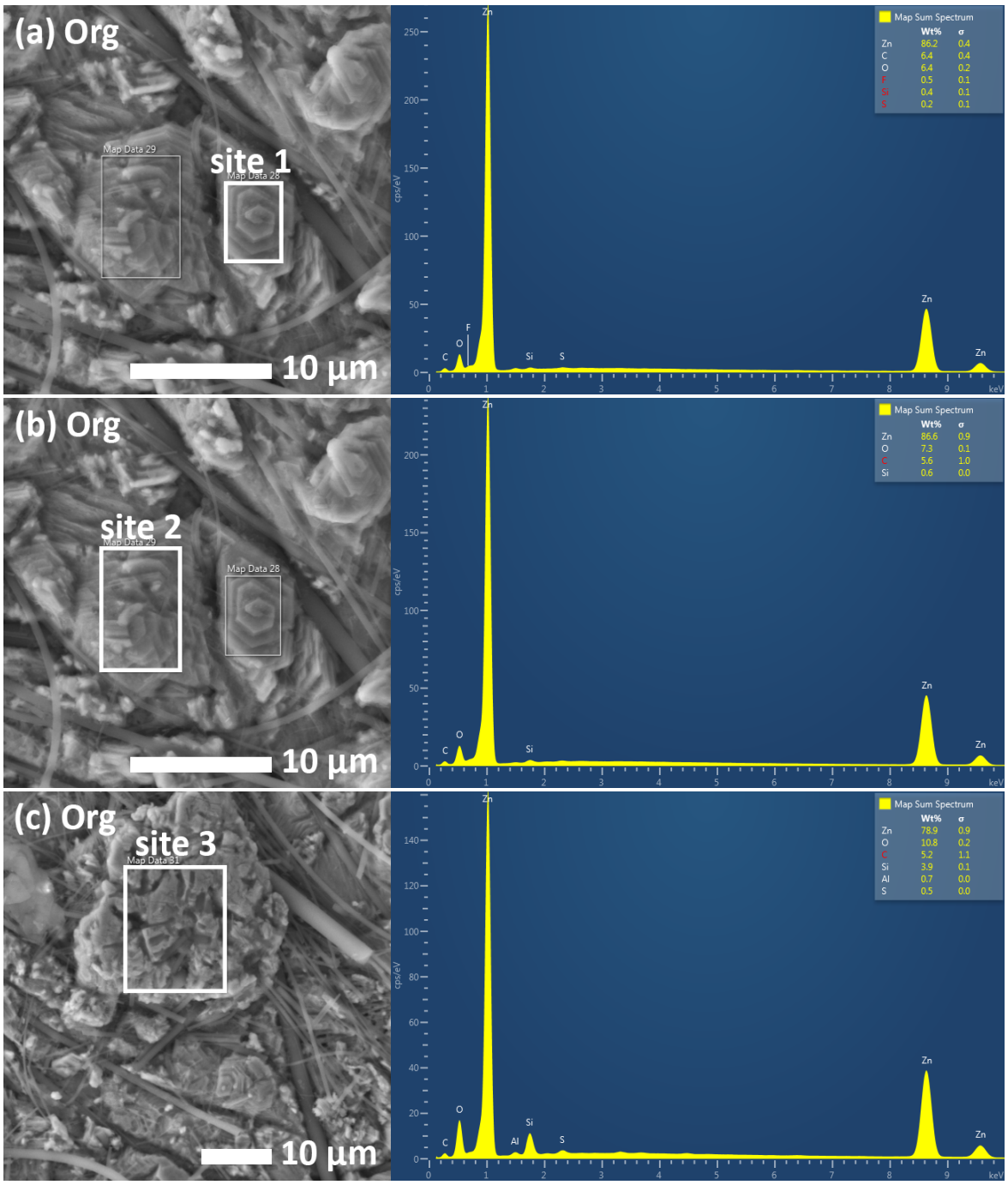

Figure S26. EDS images of Zn foil obtained from an Org ZIC (232 cycles, 1 A/g, 0.2-2 V).

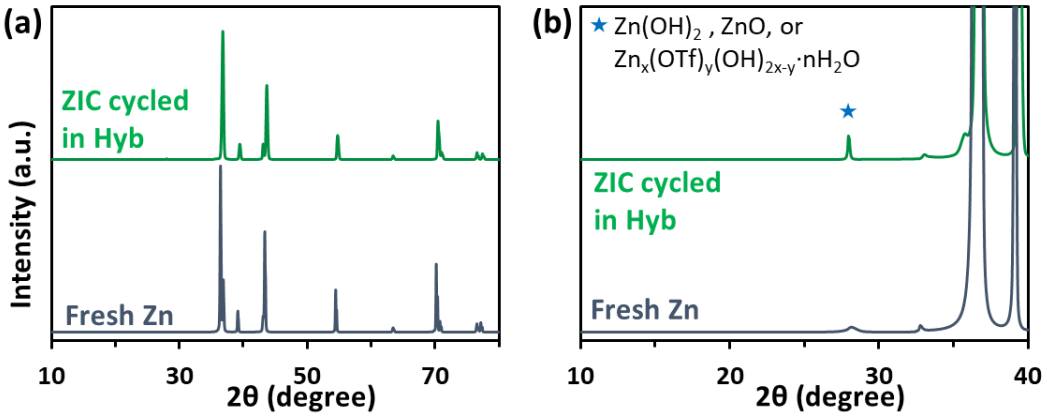

Figure S27. (a) XRD patterns of fresh Zn and Zn anode of a Hyb ZIC after 200 cycles in the range of 0.2-2V. (b) Magnified XRD patterns. The tiny new peak on the Zn surface of the Hyb sample could be attributed to $Zn(OH)_2$, ZnO, or $Zn_x(OTf)_y(OH)_{2x-y}{\cdot}nH_2O$.

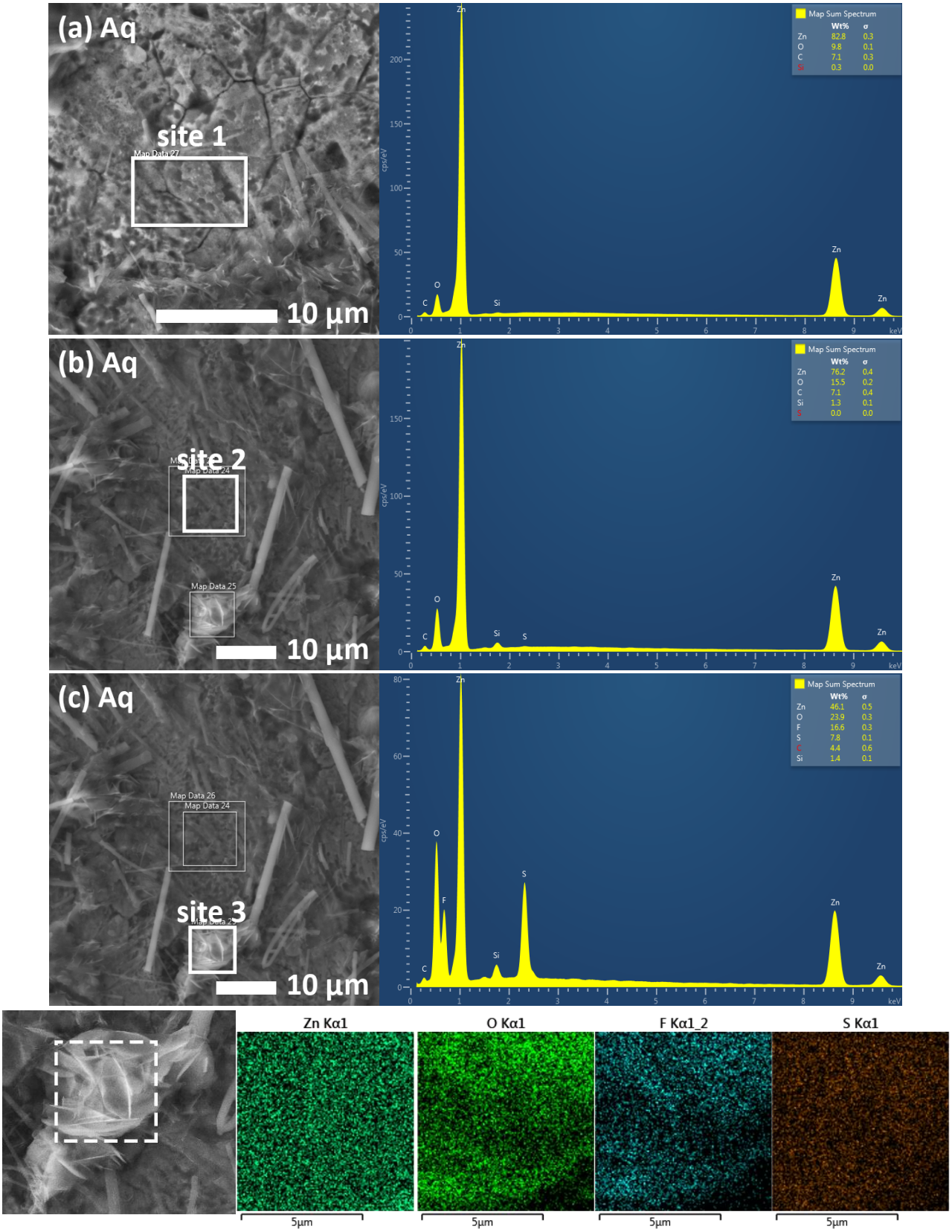

Figure S28. EDS images of Zn foil obtained from an Aq ZIC (63 cycles of rate tests, 0.2-1.8 V).

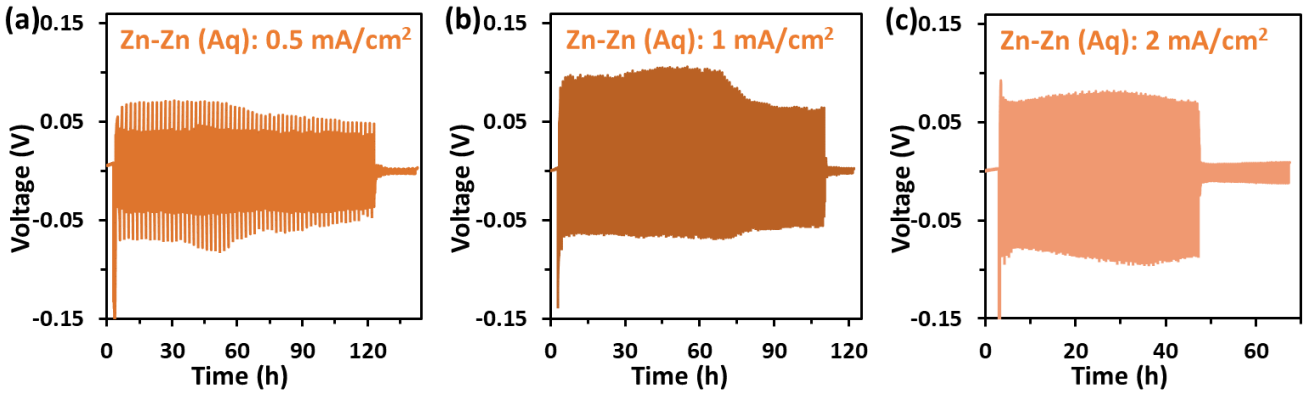

Figure S29. The voltage-time profiles of Zn-Zn symmetrical cells using the Aq electrolyte recorded at various current densities with an areal capacity of 0.5 mAh/cm^2. Two identical Zn foils (diameter: 1.4 cm), a glass fiber separator (Millipore, APFA09050), and 85 µL of the electrolyte were used in the Zn-Zn coin cells. The Zn-Zn cells with the Aq electrolyte cycled at 0.5 mA/cm^2, 1 mA/cm^2, and 2 mA/cm^2 failed after 61, 108, and 90 cycles, respectively.

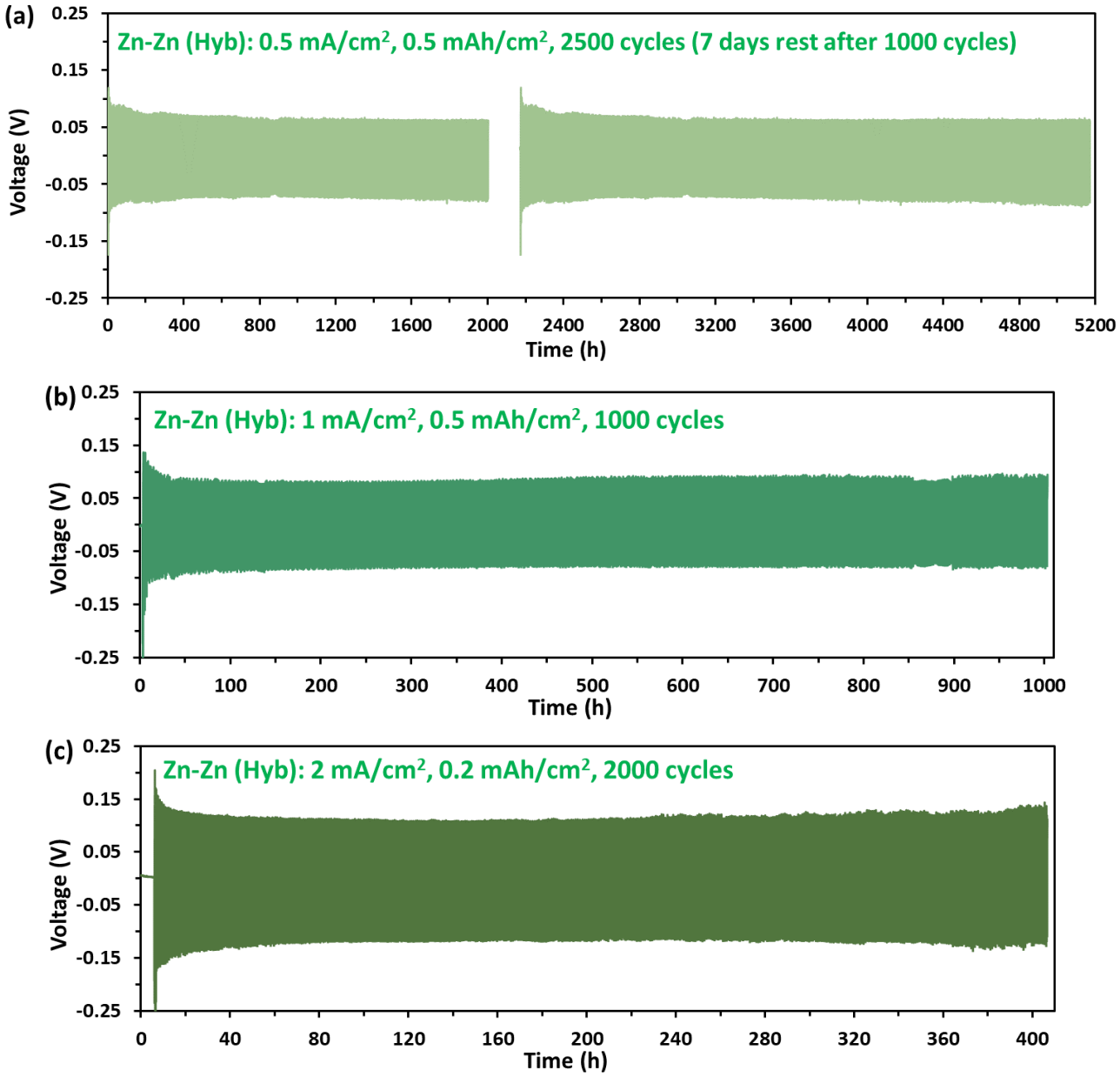

Figure S30. The voltage-time profiles of Zn-Zn symmetrical cells using the Hyb electrolyte recorded at various current densities and areal capacities. Two identical Zn foils (diameter: 1.4 cm), a glass fiber separator (Millipore, APFA09050), and 85 µL of the electrolyte were used in the Zn-Zn coin cells.

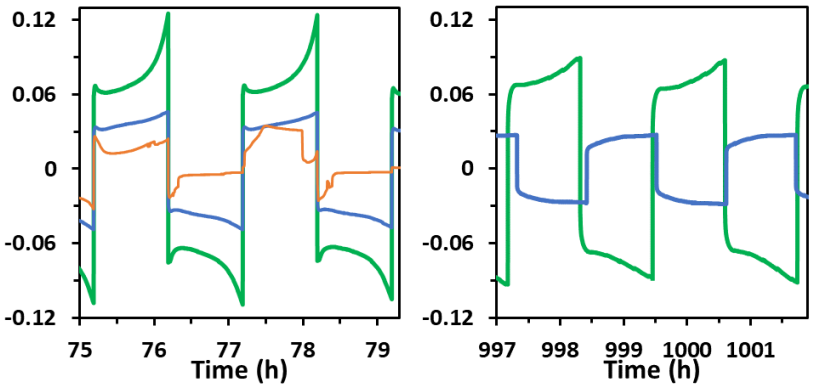

Figure S31. The enlarged voltage-time profiles of Zn-Zn symmetrical cells, shown in Figure 5a. Two identical Zn foils (diameter: 1.4 cm), a glass fiber separator (Whatman® glass microfiber, Grade GF/A), and 90 µL of the electrolyte were used in these Zn-Zn coin cells.

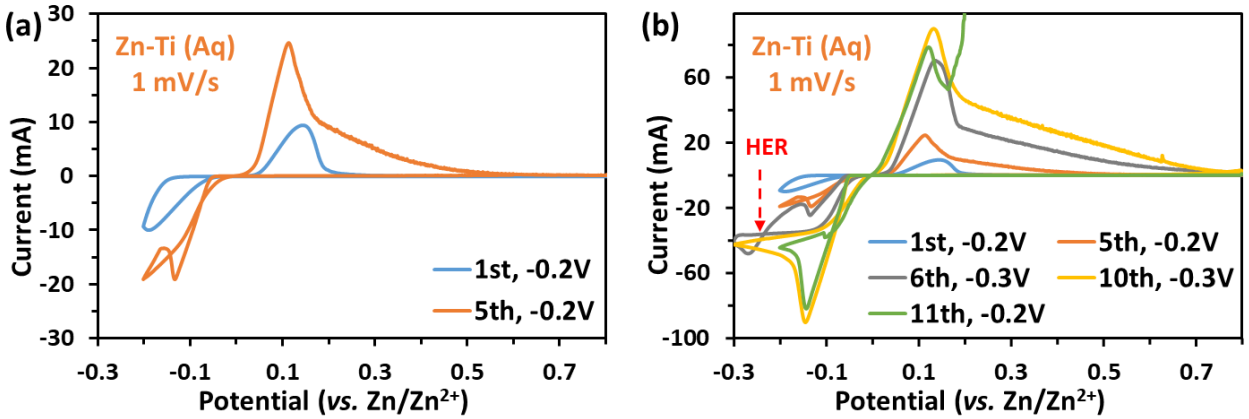

Figure S32. CV curves of an Aq Zn-Ti coin cell at 1 mV/s in the ranges of -0.2-0.8 V and -0.3-0.8 V (vs Zn/Zn^{2+}). The CV test was carried out down to -0.2 V for 5 cycles, followed by another 5 cycles down to -0.3 V. Finally, the 11^{th} cycle was performed down to -0.2 V, at which the cell failed. The constant increase of the current during the cycling is an indication of the instability caused by the competitive HER that coexists during Zn deposition. Upon going to -0.3 V, the rate of HER was further increased as identified by the red arrow in the plot.

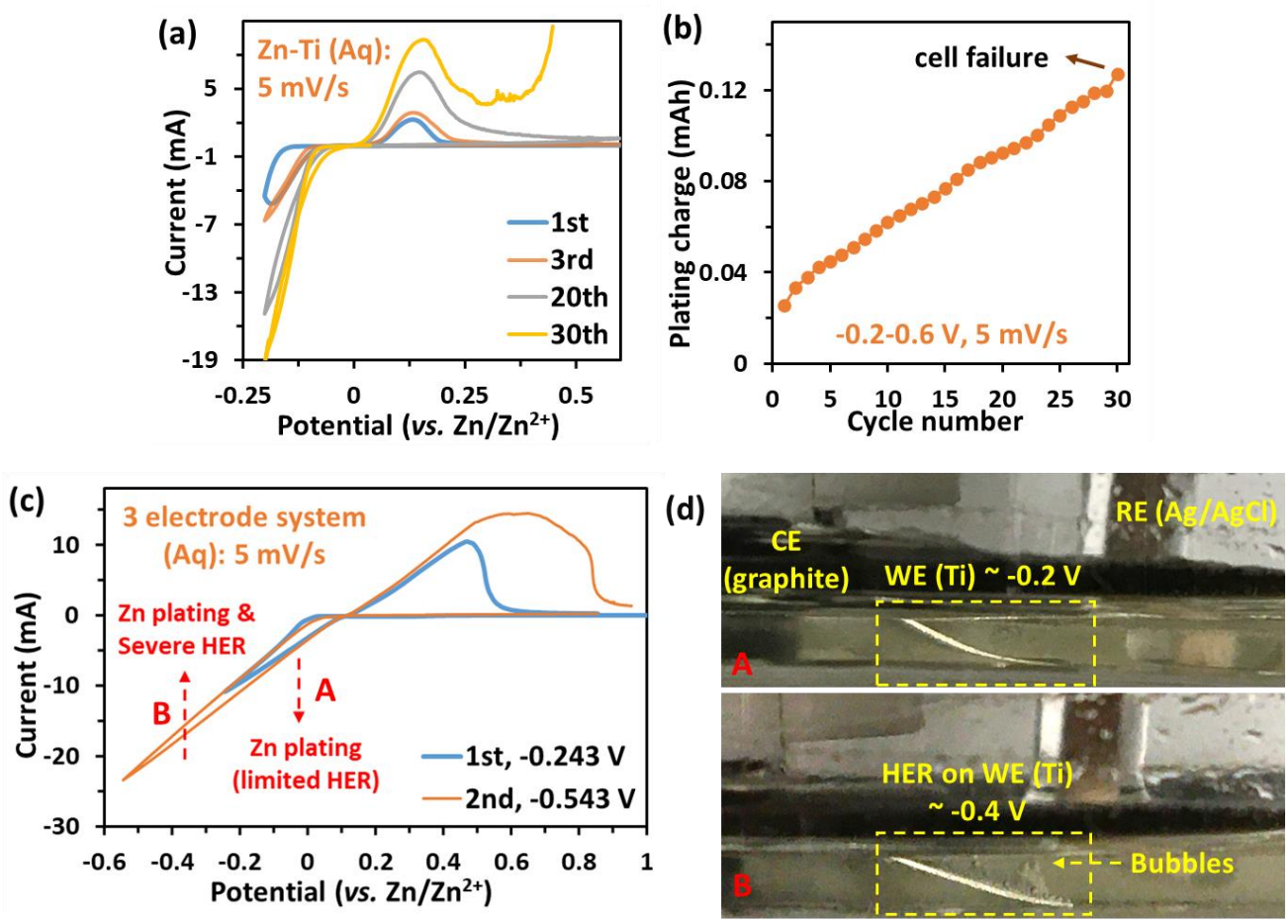

Figure S33. (a) CV curves of an Aq Zn-Ti coin cell in the range of -0.2-0.6 V at 5 mV/s and (b) the plated charge calculated from CV curves in a (area under *I-t* curves during plating). (c) CV curves in a three-electrode cell containing the Aq electrolyte at 5 mV/s using Ti working electrode, graphite rod counter electrode, and saturated Ag/AgCl reference electrode. (d) The photo of the cell in (c) at two representative potentials, i.e., A ~-0.2 V and B ~-0.4V vs Zn/Zn^{2+}, where H_2 bubbling is observed on the working electrode (WE) when the cell is scanned beyond -0.243 V. The potential of Ag/AgCl electrode was assumed to be 0.957 V vs Zn/Zn^{2+}.

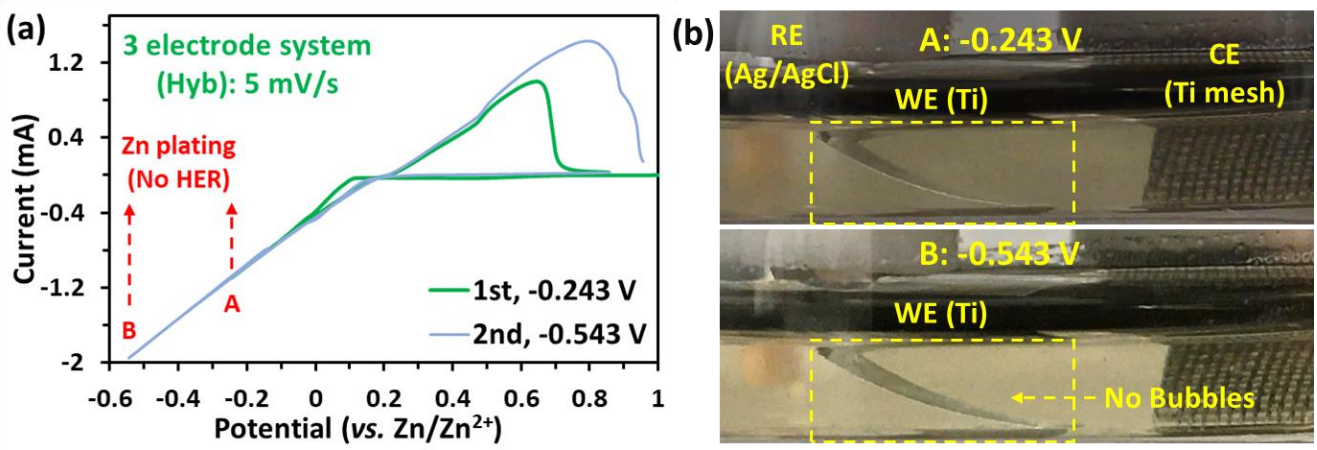

Figure S34. (a) CV curves in a three-electrode cell containing the Hyb electrolyte at 5 mV/s using Ti working electrode, Ti counter electrode, and saturated Ag/AgCl reference electrode. (b) The photo of the cell in (a) at two representative potentials, i.e., A ~-0.243 V and B ~-0.543V vs Zn/Zn^{2+}, where no H_2 bubbling is observed on the WE during Zn plating. The potential of Ag/AgCl electrode was assumed to be 0.957 V vs Zn/Zn^{2+}.

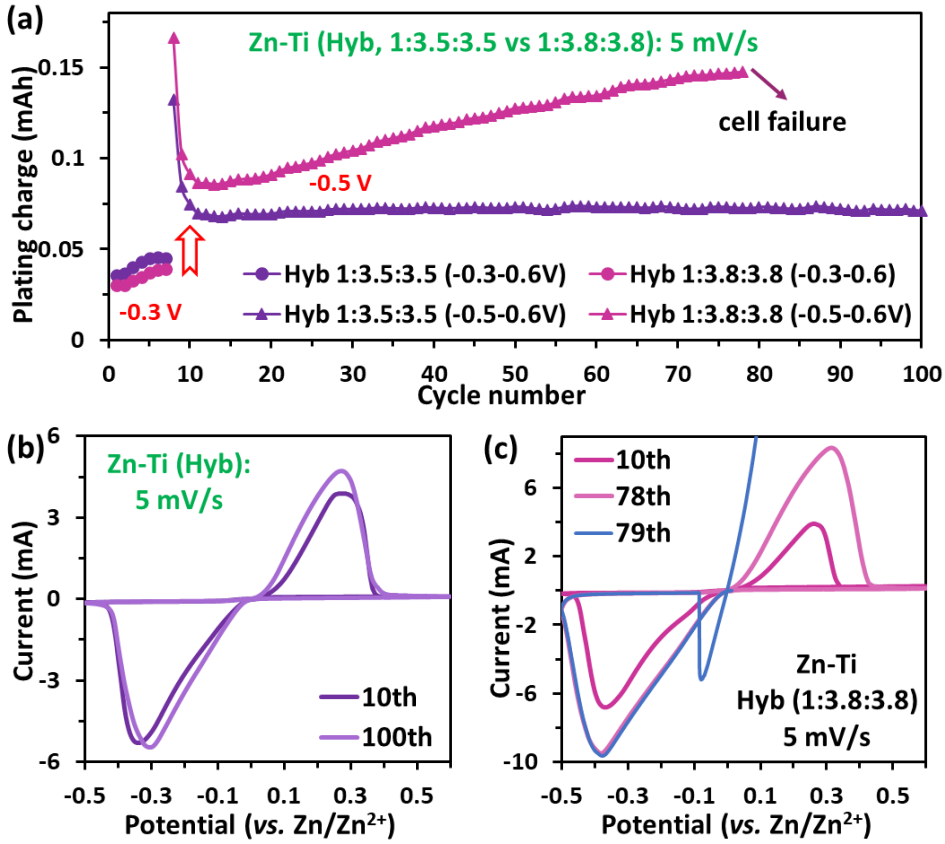

Figure S35. The effect of electrolyte concentration on the stability and Zn plating/stripping using CV of Zn-Ti cells. (a) The comparison of the plated charge calculated from CV curves (area under *I-t* curves during plating) at 5 mV/s for the Hyb electrolyte and a diluted hybrid electrolyte (with molar ratio of 1:3.8:3.8). (b) Representative CV curves of the Hyb Zn-Ti cell in the range of -0.5-0.6 V at 5 mV/s. (c) Representative CV curves of the Zn-Ti cell with a diluted hybrid electrolyte (molar ratio of 1:3.8:3.8) in the range of -0.5-0.6 V at 5 mV/s.

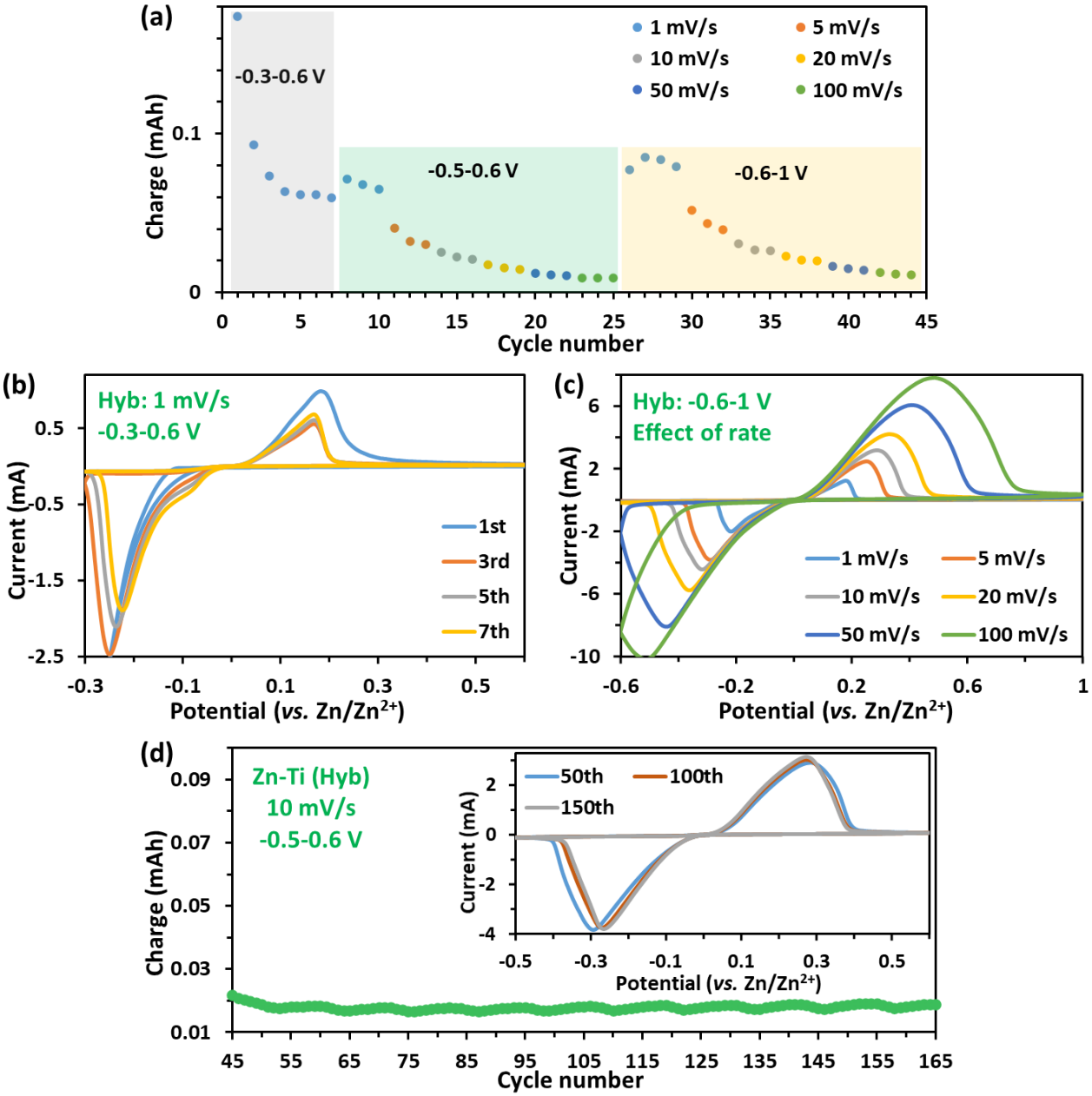

Figure S36. The stability and rate-dependency of Zn plating/stripping process in a Zn-Ti cell with the Hyb electrolyte. (a) The plated charge calculated from the CV curves of the Zn-Ti cell for different rates and voltage ranges (the area under *I-t* curves). (b) CV curves in the range of -0.3-0.6 V at 1 mV/s. (c) CV curves of the Zn-Ti cell in the voltage range of -0.6-1 V for different rates (also shown in (a) as cycles: 29, 32, 35, 38, 41, and 44). (d) The plated charge per cycle based on the CV curves of the Zn-Ti cell at 10 mV/s (inset shows the representative CV curves).

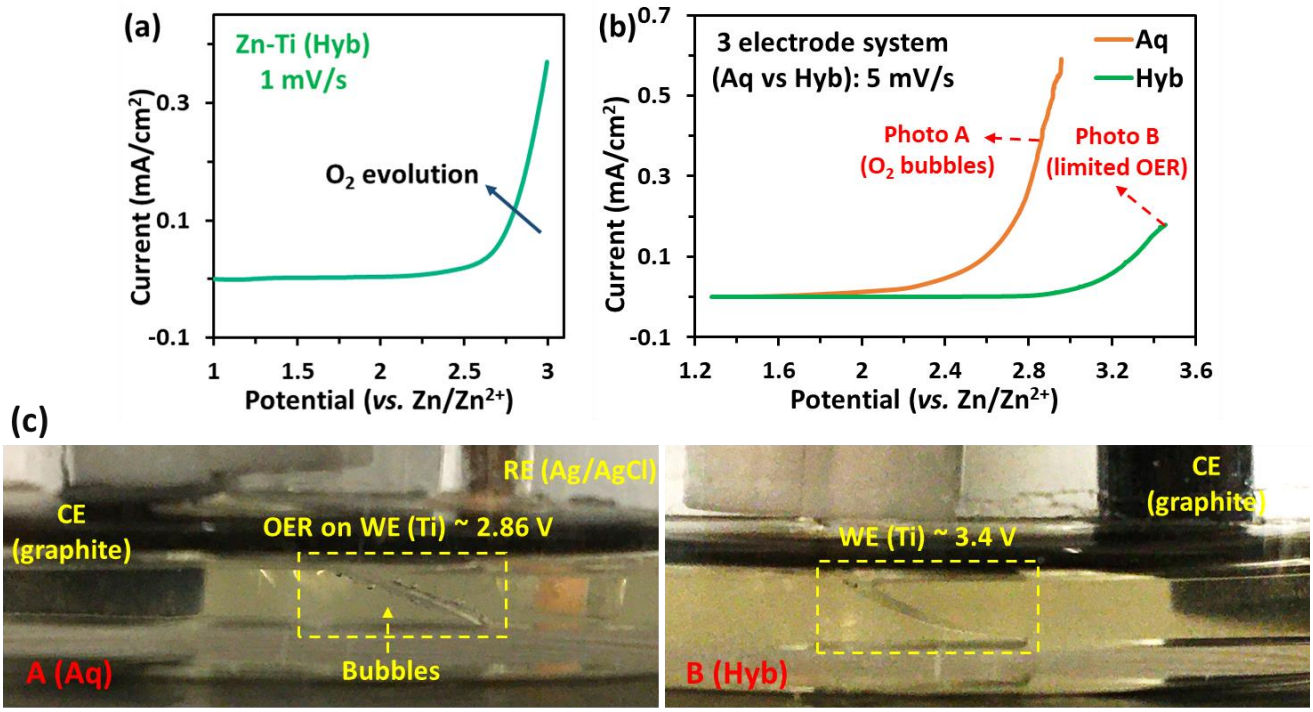

Figure S37. (a) The anodic stability of the Hyb electrolyte using a Zn-Ti coin cell at the scan rate of 1 mV/s. (b) The linear sweep voltammetry (LSV) in three-electrode cells at 5 mV/s using Ti working electrode, graphite counter electrode, and a saturated Ag/AgCl reference electrode (the potential of Ag/AgCl electrode was assumed to be 0.957 V vs Zn/Zn^{2+}.). (c) The photo of the cells in (b) at representative potentials.

The anodic process above 2.7 V (vs Zn/Zn^{2+}) is assigned to the OER on the Ti foil (0.05 mA/cm^2 is taken as the OER threshold) in the Hyb Zn-Ti cell (Figure S37a). The LSV test of the Hyb electrolyte in the three-electrode cell at 5 mV/s shows even a higher anodic stability of 3.17 V (vs Zn/Zn^{2+}), which is partly due to a higher scan rate (1 vs 5 mV/s). Nevertheless, it is noted that LSV tests of an electrolyte in the three-electrode cell often overestimates the cathodic and anodic potential limit. Thus, the Zn-Ti configuration in a coin cell gives a better estimation of the stability window of electrolytes used in ZICs (also coin cells). Figure S37b indicates that the superior anodic stability of the Hyb electrolyte over the Aq one. No apparent O_2 bubbles were visually noticed in the Hyb cell even up to 3.4 V (vs Zn/Zn^{2+}) due to less intensity of OER on the Ti foil (Figure S37c, part B). On the other hand, severe O_2 bubbling was visually observed in the Aq cell upon scanning beyond 2.8 V (vs Zn/Zn^{2+}) (Figure S37c, part A). An operando optical microscope could assist the observation of the O_2 bubbling with less intensity at lower potentials [27].

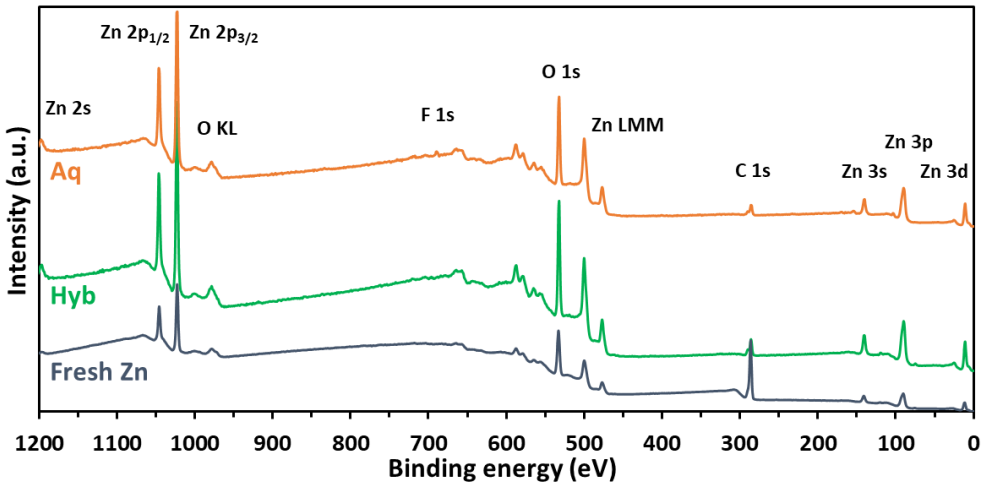

Figure S38. XPS survey spectra of Zn foils obtained from Zn-Ti cells in the Aq and Hyb electrolytes (Figure 5g) compared with that of fresh Zn foil.

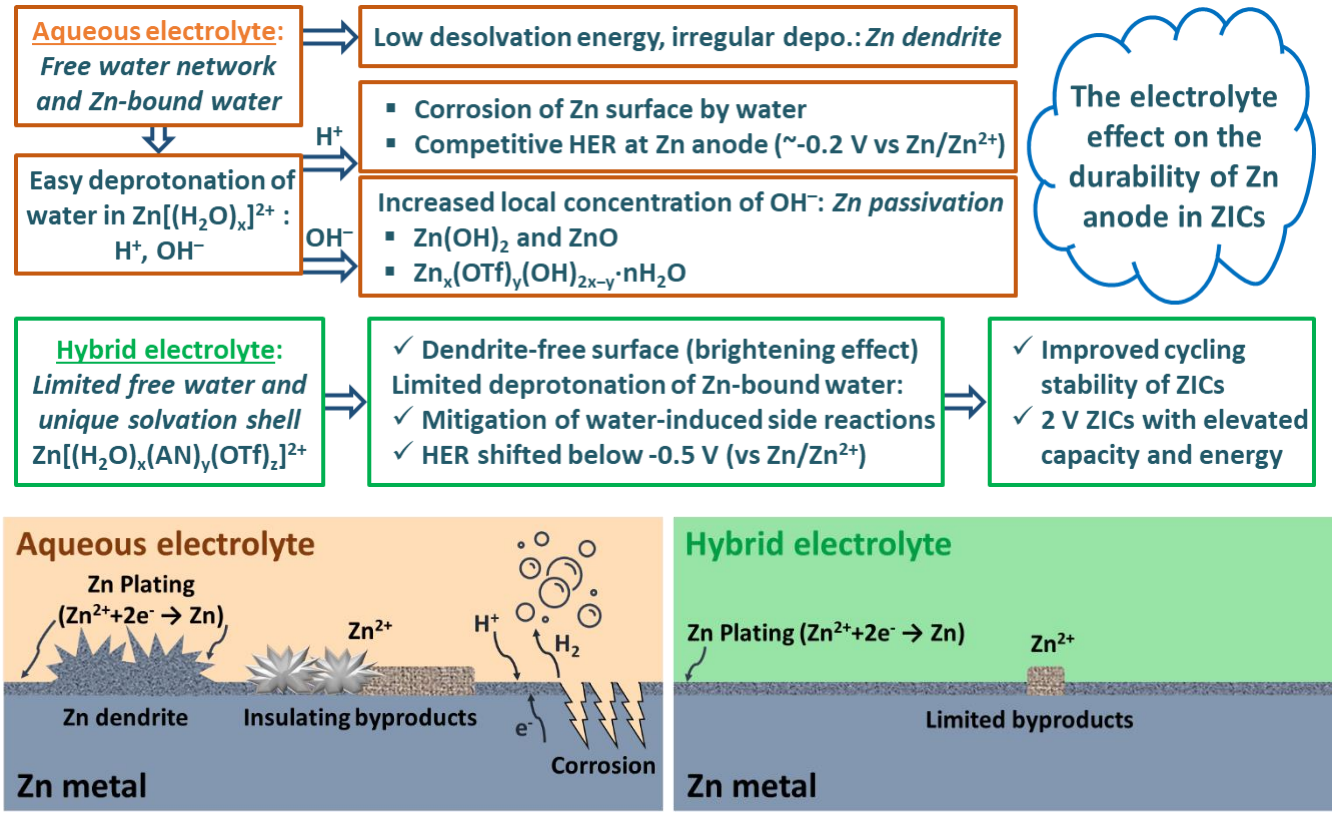

Figure S39. The effect of Aq and Hyb electrolytes on the durability of Zn anodes. The flowchart summarizes the implications of the difference in the solvation structure of Aq and Hyb (Figure 1) on the behavior of Zn anode. The schematic on the left describes the interfacial reactions between Zn anode and the Aq electrolyte. The schematic on the right shows the mitigation of such reactions in the Hyb electrolyte. This summary is based on the results presented in this work as well as the discussions on the Aq electrolyte in the literature [21, 33-35].

Performance and stability of Org ZICs at 2 V:

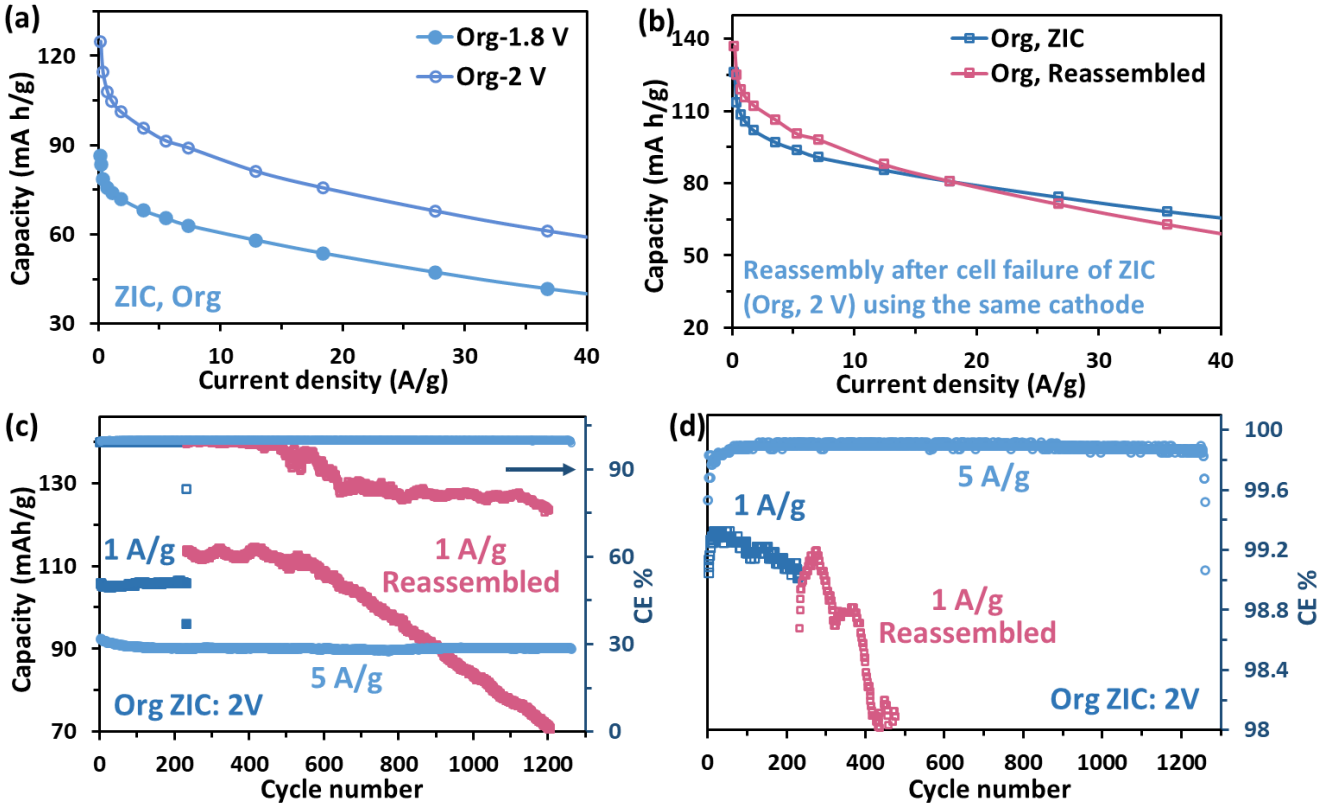

Figure S40. Electrochemical behavior of Org ZICs; (a) Specific capacity of Org ZICs at various current densities within the voltage range of 0.2-1.8 V and 0.2-2 V. The GCD curves are provided in Figure S9d and e. (b) Comparison of capacity of an Org ZIC before and after reassembly. The Org ZIC was reassembled after it died (failed after 232 cycles at 1 A/g). The same cathode but fresh electrolyte, separator, and Zn foil were used for the reassembly. (c) Cycling performance of Org ZICs within the voltage range of 0.2-2 V at 1 A/g and 5 A/g. (d) magnified CE% in (c). The mass loading of AC30 in the cathodes are 2.15 mg/cm^2 (in a and 5 A/g in c) and 2.22 mg/cm^2 (ZICs in b and 1 A/g in c).

To exclude the role of the cathode in the failure of this Org ZIC (failed after 232 cycles at 1 A/g), it was reassembled using the same cathode but with fresh electrolyte, separator, and Zn foil. The reassembled Org ZIC showed slightly higher capacity at low currents, but an inferior rate performance compared with the original ZIC (Figure S40b). This could be due to residual salts remained in the cathode and/or a slight change in the density of the cathode during coin cell disassembly and reassembly. Upon cycling in the range of 0.2-2 V at 1 A/g, the reassembled Org ZIC maintained its capacity for about 340 cycles before fading rapidly likely due to the electrolyte drainage (Figure S40c).

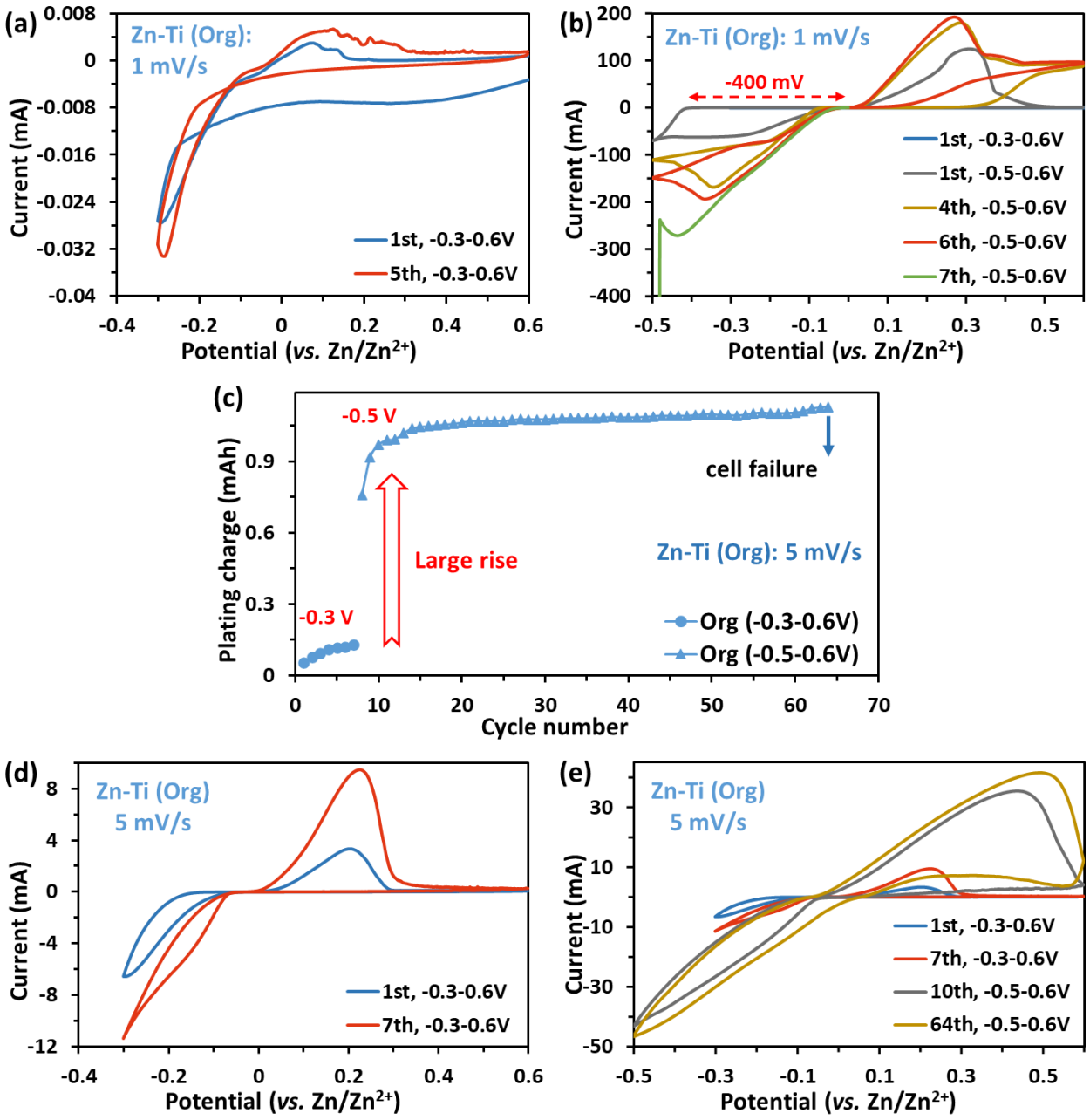

Figure S41. Zn plating/stripping in the Org electrolyte using CV tests on Zn-Ti coin cells. CV curves of Org Zn-Ti cells at 1 mV/s in the voltage range of (a) -0.3-0.6 V and (b) -0.5-0.6 V. (b) The plated charge calculated from CV curves at 5 mV/s (area under *I-t* curves during plating). CV curves at 5 mV/s in the voltage range of (a) -0.3-0.6 V and (b) -0.5-0.6 V.

Similar potential-dependent plating/stripping of Zn is observed for an Org Zn-Ti cell undergoing voltammetric tests at 5 mV/s. According to Figure S41 c-e, decreasing the plating voltage from -0.3 V to -0.5 V results in a large rise to the plating charge (and stripping), which is much greater than that of the Hyb cell tested at the same condition (Figure S35). The continuous increase of the charge (instability)

during the voltammetric cycling in the range of -0.5-0.6 V for 1 mV/s is not taking place for 5 mV/s. Nevertheless, the Org Zn-Ti cell failed after 64 cycles at 5 mV/s likely due to the Zn or electrolyte drainage considering large plating/stripping charges (Figure S41c). This data (1 vs 5 mV/s) also suggests that water contamination of Org is more damaging at a low rate.

References

1. T. D. Kühne, M. Iannuzzi, M. D. Ben, V. V. Rybkin, P. Seewald, F. Stein, T. Laino, R. Z. Khaliullin, O. Schütt, F. Schiffmann, D. Golze, J. Wilhelm, S. Chulkov, M. H. Bani-Hashemian, V. Weber, U. Borštnik, M. Taillefumier, A. S. Jakobovits, A. Lazzaro, H. Pabst, T. Müller, R. Schade, M. Guidon, S. Andermatt, N. Holmberg, G. K. Schenter, A. Hehn, A. Bussy, F. Belleflamme, G. Tabacchi, A. Glöß, M. Lass, I. Bethune, C. J. Mundy, C. Plessl, M. Watkins, J. VandeVondele, M. Krack and J. Hutter, *J. Chem. Phys.*, 2020, **152**, 194103.
2. J. VandeVondele and J. Hutter, *J. Chem. Phys.*, 2007, **127**, 114105.
3. C. Hartwigsen, S. Goedecker and J. Hutter, *Phys. Rev. B*, 1998, **58**, 3641-3662.
4. J. Cheng, M. Sulpizi and M. Sprik, *J. Chem. Phys.*, 2009, **131**, 154504.
5. A. Baskin and D. Prendergast, *J. Phys. Chem. Lett.*, 2019, **10**, 4920-4928.
6. R. Qin, Y. Wang, M. Zhang, Y. Wang, S. Ding, A. Song, H. Yi, L. Yang, Y. Song, Y. Cui, J. Liu, Z. Wang, S. Li, Q. Zhao and F. Pan, *Nano Energy*, 2021, **80**, 105478.
7. M. Sevilla and A. B. Fuertes, *ACS Nano*, 2014, **8**, 5069-5078.
8. Q. Wang, J. Yan and Z. Fan, *Energy Environ. Sci.*, 2016, **9**, 729-762.
9. A. Khosrozadeh, L. Tao, P. Zhao, M. B. Miller, O. Voznyy and J. Liu, *J. Power Sources*, 2021, **498**, 229905.
10. Q. Yang, G. Liang, Y. Guo, Z. Liu, B. Yan, D. Wang, Z. Huang, X. Li, J. Fan and C. Zhi, *Adv. Mater.*, 2019, **31**, 1903778.
11. G.-H. An, J. Hong, S. Pak, Y. Cho, S. Lee, B. Hou and S. Cha, *Adv. Energy Mater.*, 2020, **10**, 1902981.
12. S. Wu, Y. Chen, T. Jiao, J. Zhou, J. Cheng, B. Liu, S. Yang, K. Zhang and W. Zhang, *Adv. Energy Mater.*, 2019, **9**, 1902915.
13. H. Zhou, C. Liu, J.-C. Wu, M. Liu, D. Zhang, H. Song, X. Zhang, H. Gao, J. Yang and D. Chen, *J. Mater. Chem. A*, 2019, **7**, 9708-9715.
14. H. Zhang, Q. Liu, Y. Fang, C. Teng, X. Liu, P. Fang, Y. Tong and X. Lu, *Adv. Mater.*, 2019, **31**, 1904948.
15. Z. Zhou, X. Zhou, M. Zhang, S. Mu, Q. Liu and Y. Tang, *Small*, 2020, **16**, 2003174.
16. H. Wang, C. Zhu, D. Chao, Q. Yan and H. J. Fan, *Adv. Mater.*, 2017, **29**, 1702093.
17. M. Yu, D. Lin, H. Feng, Y. Zeng, Y. Tong and X. Lu, *Angew. Chem. Int. Ed.*, 2017, **56**, 5454-5459.
18. L. Dong, X. Ma, Y. Li, L. Zhao, W. Liu, J. Cheng, C. Xu, B. Li, Q.-H. Yang and F. Kang, *Energy Storage Mater.*, 2018, **13**, 96-102.
19. P. Yu, Y. Zeng, Y. Zeng, H. Dong, H. Hu, Y. Liu, M. Zheng, Y. Xiao, X. Lu and Y. Liang, *Electrochim. Acta*, 2019, **327**, 134999.
20. Y. Lu, Z. Li, Z. Bai, H. Mi, C. Ji, H. Pang, C. Yu and J. Qiu, *Nano Energy*, 2019, **66**, 104132.
21. Z. Wang, J. Huang, Z. Guo, X. Dong, Y. Liu, Y. Wang and Y. Xia, *Joule*, 2019, **3**, 1289-1300.

22. J. Yin, W. Zhang, W. Wang, N. A. Alhebshi, N. Salah and H. N. Alshareef, *Adv. Energy Mater.*, 2020, **10**, 2001705.
23. H. Wang, M. Wang and Y. Tang, *Energy Storage Mater.*, 2018, **13**, 1-7.
24. S. Chen, L. Ma, K. Zhang, M. Kamruzzaman, C. Zhi and J. A. Zapien, *J. Mater. Chem. A*, 2019, **7**, 7784-7790.
25. N. Chang, T. Li, R. Li, S. Wang, Y. Yin, H. Zhang and X. Li, *Energy Environ. Sci.*, 2020, **13**, 3527-3535.
26. F. Wang, O. Borodin, T. Gao, X. Fan, W. Sun, F. Han, A. Faraone, J. A. Dura, K. Xu and C. Wang, *Nat. Mater.*, 2018, **17**, 543-549.
27. J. Zhao, J. Zhang, W. Yang, B. Chen, Z. Zhao, H. Qiu, S. Dong, X. Zhou, G. Cui and L. Chen, *Nano Energy*, 2019, **57**, 625-634.
28. S. Chen, R. Lan, J. Humphreys and S. Tao, *Energy Storage Mater.*, 2020, **28**, 205-215.
29. Q. Ni, H. Jiang, S. Sandstrom, Y. Bai, H. Ren, X. Wu, Q. Guo, D. Yu, C. Wu and X. Ji, *Adv. Funct. Mater.*, 2020, **30**, 2003511.
30. L. Zhang, I. A. Rodríguez-Pérez, H. Jiang, C. Zhang, D. P. Leonard, Q. Guo, W. Wang, S. Han, L. Wang and X. Ji, *Adv. Funct. Mater.*, 2019, **29**, 1902653.
31. X. Song, H. He, M. H. Aboonasr Shiraz, H. Zhu, A. Khosrozadeh and J. Liu, *Chem. Commun.*, 2021, **57**, 1246-1249.
32. G. Fang, C. Zhu, M. Chen, J. Zhou, B. Tang, X. Cao, X. Zheng, A. Pan and S. Liang, *Adv. Funct. Mater.*, 2019, **29**, 1808375.
33. Y. Zhang, Z. Chen, H. Qiu, W. Yang, Z. Zhao, J. Zhao and G. Cui, *NPG Asia Materials*, 2020, **12**, 4.
34. Z. Cao, P. Zhuang, X. Zhang, M. Ye, J. Shen and P. M. Ajayan, *Adv. Energy Mater.*, 2020, **10**, 2001599.
35. C. Han, W. Li, H. K. Liu, S. Dou and J. Wang, *Nano Energy*, 2020, **74**, 104880.